A staggered scheme for the compressible Euler equations on general 3D meshes

Aubin Brunel, Raphaèle Herbin, Jean-Claude Latché

A STAGGERED SCHEME FOR THE COMPRESSIBLE EULER EQUATIONS ON GENERAL 3D MESHES

Aubin Brunel[1], Raphaèle Herbin[2] and Jean-Claude Latché[3]

Abstract. We address here the discretization of the momentum convection operator for fluid flow simulations on 2D triangular and quadrangular meshes and 3D polyhedral meshes containing hexahedra, tetrahedra, prisms and pyramids. The finite volume scheme that we use for the full Euler equations is based on a staggered discretization: the density unknowns are associated with a primal mesh, whereas the velocity unknowns are associated with a "fictive" dual mesh. Accordingly, the convection operator of the mass balance equation is derived on the primal mesh, while the the convection operator of the momentum balance equation is discretized on the dual mesh. To avoid any hazardous interpolation of the unknowns on a possibly ill-defined dual mesh, the mass fluxes of the momentum convection operator are computed from the mass fluxes of the mass balance equation, so as to ensure the stability of the resulting operator. A coherent reconstruction of these dual fluxes is possible, based only on the kind of considered polygonal or polyhedral cell, and not on each cell itself. Moreover, we show that this process still yields a consistent convection operator in the Lax-Wendroff sense, that is, if a sequence of piecewise constant functions is supposed to converge to a a given limit, then the weak form of the corresponding discrete convection operator converges to the weak form of the continuous operator applied to this limit. The derived discrete convection operator applies to both constant and variable density flows and may thus be implemented in a scheme for incompressible or compressible flows. Numerical tests are performed for the Euler equations on several types of mesh, including hybrid meshes, and show the excellent performance of the method.

2020 AMS Subject Classification. 65M08, 76M12.

.

We address in this paper a numerical scheme for the Euler equations, which read:

$$\partial_t \rho + \mathrm{div}(\rho\, \boldsymbol{u}) = 0, \tag{1a}$$

$$\partial_t (\rho\, u_i) + \mathrm{div}(\rho\, u_i\, \boldsymbol{u}) + \partial_i p = 0, \quad 1 \le i \le d, \tag{1b}$$

$$\partial_t (\rho\, E) + \mathrm{div}(\rho\, E\, \boldsymbol{u}) + \mathrm{div}(p\, \boldsymbol{u}) = 0, \tag{1c}$$

$$p = (\gamma - 1)\, \rho\, e, \qquad E = \frac{1}{2}|\boldsymbol{u}|^2 + e, \tag{1d}$$

where the quantities $\boldsymbol{u}$, ρ, p, E and e refer respectively to the velocity of the fluid, its density, its pressure, the total energy and the internal energy, and γ is a coefficient specific to the fluid and is supposed strictly greater than 1. The problem is supposed to be posed over a spatial domain Ω and on a time interval $[0, T]$, where Ω is an open bounded connected subset of $\mathbb{R}^d$ with $1 \le d \le 3$. The system is supplemented by the following initial conditions:

$$\rho(\boldsymbol{x}, 0) = \rho_0(\boldsymbol{x}),\ \boldsymbol{u}(\boldsymbol{x}, 0) = \boldsymbol{u}_0(\boldsymbol{x}),\ \text{with } \rho_0 \in L^\infty(\Omega), \boldsymbol{u}_0 \in L^\infty(\Omega)^d, \tag{2}$$

Keywords and phrases: Staggered discretizations, Momentum convection operator, Finite volume, Euler equations, Compressible flows

[1] Aix-Marseille University, CNRS, France (aubin.brunel@univ-amu.fr)

[2] Aix-Marseille University, CNRS, France (raphaele.herbin@univ-amu.fr)

[3] Institut de Sûreté et de Radioprotection Nucléaire (IRSN), France (jean-claude.latche]@irsn.fr)

and suitable boundary conditions.

In a previous paper [10] co-signed by two of the above authors, a staggered in space and segregated in time scheme, involving only explicit steps, was developed to approximate the solutions of the Euler equations on general simplicial or quadrilateral/hexahedral meshes. Our aim in the present work is twofold: first we generalize the scheme to prismatic and pyramidal meshes and give a precise definition of the convective fluxes for these cells; second, we give a proof of the Lax-Wendroff consistency of the scheme for general meshes, in the sense that if a sequence of approximate solutions is assumed to converge to a certain limit as the time and space steps tend to zero, then this limit is necessarily a weak solution of the Euler equations.

Let us first recall the essential features of the proposed numerical scheme.

- The scheme features a staggered arrangement of the unknowns: the scalar variables (density, pressure) are approximated by piecewise constant functions over the cells while the velocity is approximated at the faces of the cells.
- The equations are discretized by a finite volume scheme.
- Although not fully explicit, the scheme is segregated and each step is explicit, in the sense that the balance equations are solved successively and do not require any linear system solver.
- The scheme solves the internal energy balance rather than the total energy balance, and thus conserves the positivity of the internal energy; a corrective term is added in this equation in order to avoid wrong shock solutions.
- Upwinding or more precise procedures are avalaible for the convection fluxes, which ensures the positivity of the density, internal energy and pressure.

The scheme is related to the family of flux splitting schemes of the references [15,16,19,21,22]. However it differs from them because of the use of staggered discretization which has the advantage of providing a discrete inf-sup stability condition, and by the use of the internal energy equation. Moreover, the pressure gradient is discretized as the dual of the velocity divergence, which, coupled with the preservation of the positivity of the density, yields a discrete analogue of the conservation of the total energy. The continuous mass balance equation (1a) is discretized on a primal mesh, whereas the momentum convection operator for the i-th component of the velocity (with $1 \leq i \leq d$, where d is the dimension of the problem), given by

$$(\mathcal{C}u)_i := \partial_t(\rho\, u_i) + \mathrm{div}(\rho\, u_i\, \boldsymbol{u}), \tag{3}$$

is discretized on the dual mesh. As a consequence, the mass fluxes are first defined on the primal mesh and the densities and mass fluxes are reconstructed on the dual mesh from the primal mesh densities and mass fluxes respectively, so as to ensure that a mass balance holds on the dual cells; this is a crucial step to ensure the L^2-stability of the scheme, see e.g. [7].

The first goal of this paper is to propose a general reconstruction method of these dual cell mass fluxes (and thus, of the momentum convection operator) on a wide range of cells, including prismatic and pyramidal cells in 3D, which are often encountered in industrial meshes. Indeed, industrial 3D meshes are often based on both hexahedral and tetrahedral elements cells, and the usual way to connect a tetraheda to a heaxhedra is to use pyramids or prisms [3,4,17,18,20]. The scientific software CALIF3S [6] that is routinely used at IRSN for nuclear safety studies supports the use of hybrid tetrahedral-hexahedral-prismatic-pyramidal meshes.

In the present work, we generalize the reconstruction of the dual fluxes from the primal fluxes which was introduced for simplicial and hexahedral meshes (see e.g. [10, 11]) to these hybrid meshes, and the requirement of a local mass balance equation leads to the problem of the resolution linear system. The resulting system that needs to be solved for this reconstruction may be underdetermined; a procedure is constructed in order to find a solution of the system for a given polygon or polyhedron, regardless of its possible distorsion or anisotropy.

The construction of the dual fluxes is thus based on a set of algebraic equations, rather than on integration on some well defined control volume; this might seem unorthodox in the framework of the finite volume method. However, to support the validity of this method, we give a general consistency result: this is the second goal of the paper. Indeed, we show that the derived discrete convection operator is weakly consistent in the Lax-Wendroff sense, *i.e.* that its weak form tends to the weak form of the continuous convection operator as the space and time steps both tend to 0.

The paper is organized as follows. In section 1, we give the time and space discretizations. The mesh definition is given such as to take into account several kinds of grid cells in two or three space dimensions. Section 2 is devoted to the definition of the scheme, with special emphasis on the construction of the convection operator and its link with the mass balance equation, which is the subject of Section 3. In the case of pyramidal and prismatic cells, the linear systems satisfied by the dual fluxes are underdetermined; we give the specific choice of a solution that is implemented in the code. The scheme is shown to be consistent in the Lax-Wendroff sense in section 4. The behaviour of the numerical scheme on some test cases is investigated in section 5. Finally, some lemmas needed for the Lax-Wendroff consistency are recalled in the appendix.

1. Space and time discretization

Due to the staggered nature of the scheme, the discretization consists in a primal mesh and a dual mesh that is derived from the primal one. We therefore first define the primal mesh $\mathcal{M}$, which is obtained by splitting the domain Ω into a finite family of disjoint polygons (triangles and quadrangles) when $d = 2$ and polyhedra (hexahedra, tetrahedra, prisms and pyramids) when $d = 3$. Following, we will refer to a primal element as a control volume or a cell. The set of the faces (if $d = 3$, or edges if $d = 2$) of the mesh is denoted by $\mathcal{E}$. It is split into $\mathcal{E} = \mathcal{E}_{\rm int} \cup \mathcal{E}_{\rm ext}$, where $\mathcal{E}_{\rm ext}$ is the set of external faces (or edges) and $\mathcal{E}_{\rm int}$ is the set of internal faces (or edges), that we define as follows. A face (or edge) $\sigma \in \mathcal{E}$ is said to be an external face (or edge), and thus $\sigma \in \mathcal{E}_{\rm ext}$, if it is part of the boundary of the domain (*i.e.* $\sigma \subset \partial\Omega$), whereas $\sigma \in \mathcal{E}$ is said to be an internal face (or edge), and thus $\sigma \in \mathcal{E}_{\rm int}$, if there exists $(K, L) \in \mathcal{M}^2$ with $K \neq L$ such that $\overline{K} \cap \overline{L} = \sigma$. Such a face (or edge) is thus denoted $\sigma = K|L$. Moreover, for $K \in \mathcal{M}$ and $\sigma \in \mathcal{E}$, we denote by $|K|$ the measure of K and $|\sigma|$ the $(d-1)$-measure of σ.

Then, the dual mesh is constructed as follows: for a regular polygon or a regular polyhedron $K \in \mathcal{M}$, we denote by $\boldsymbol{x}_K$ the mass center of K and we construct $D_{K,\sigma}$ as the cone with basis σ and with vertex $\boldsymbol{x}_K$; this definition is extended to a general cell K, by supposing that K is split in the same number of sub-cells (the geometry of which does not need to be specified) and with the same connectivity. We can now define for each $\sigma \in \mathcal{E}$ its associated dual cells D_σ. When $\sigma \in \mathcal{E}_{\rm int}$ with $\sigma = K|L$, we define $D_\sigma := D_{K,\sigma} \cup D_{L,\sigma}$; if $\sigma \in \mathcal{E}_{\rm ext} \cap \mathcal{E}(K)$, then we have $D_\sigma := D_{K,\sigma}$. We then denote by $\tilde{\mathcal{E}}(D_\sigma)$ the set of dual faces (or edges) of D_σ, and by $\epsilon = D_\sigma|D_{\sigma'}$ the face (or edge) separating two dual cells D_σ and $D_{\sigma'}$.

Next, we associate the unknowns associated with the scalar variable, such as the pressure and the density for instance, the cells of the primal mesh $\mathcal{M}$, and they are denoted in those instances by p_K and ρ_K for a cell $K \in \mathcal{M}$. On the other hand, the degrees of freedom for the velocity are linked to the dual mesh faces and are denoted $\boldsymbol{u}_\sigma = (u_{\sigma,1}, \ldots, u_{\sigma,d})$ for an edge $\sigma \in \mathcal{E}$. All the components of the velocity are thus approximated on each face of the mesh, and their degrees of freedom are identified to the mean value of the velocity component over the face.

An example of the discretization with a few control volumes is given on Figure 1.

Finally, a constant time step denoted by δt is used for the time discretization, and the discrete solution will thus be computed at each time t^n with $t^n := n\,\delta t$, for n varying between 0 and $N := \lfloor \frac{T}{\delta t} \rfloor$. An index n is then used to refer to the time step, that is to say that the unknows will be denoted by $(p_K^n)_{K\in\mathcal{M},\ 0\leq n\leq N}$, $(\rho_K^n)_{K\in\mathcal{M},\ 0\leq n\leq N}$ and $(\boldsymbol{u}_\sigma^n)_{\sigma\in\sigma,\ 0\leq n\leq N}$.

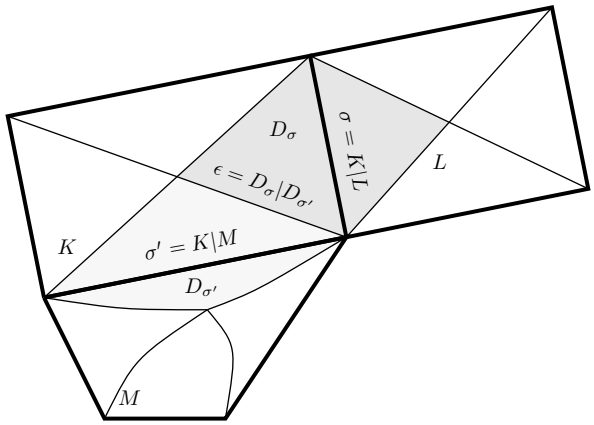

FIGURE 1. Primal and dual meshes for the Rannacher-Turek elements.

2. The numerical scheme

In the following, we will propose a scheme based on the internal energy balance formulation of the Euler equations, which reads:

$$\partial_t(\rho e) + \operatorname{div}(\rho e \boldsymbol{u}) + p \operatorname{div}\boldsymbol{u} = 0, \tag{4}$$

rather than the total energy balance (Equation (1c)). The former may be derived from the latter thanks to a kinetic energy identity obtained by taking the inner product of Equation (1b) with the velocity. Such a choice is motivated by the following reasons. First, a well-thought approximation of the convection term of Equation (4) leads to a conservation of the positivity of the internal energy, which seems difficult to obtain by a direct discretization of the the total energy balance. Second, on a staggered discretization, the total energy is a function of quantities given on both the primal and the dual mesh. A discretization of this equation may thus yield an awkward combination of those quantities, and this difficulty might be avoided by working directly with the internal energy balance.

The scheme thus takes the following form; it features several discrete operators, defined either on the primal mesh or on the dual meshes associated to the components of the velocity; these are defined in the following paragraphs.

Initialization:

$$\rho_K^0 = \frac{1}{|K|}\int_K \rho_0(\boldsymbol{x})\,\mathrm{d}\boldsymbol{x}, \qquad \boldsymbol{u}_\sigma^0 = \frac{1}{|D_\sigma|}\int_{D_\sigma} \boldsymbol{u}_0(\boldsymbol{x})\,\mathrm{d}\boldsymbol{x} \tag{5a}$$

Solve for $n \geq 0$,

$$\forall K \in \mathcal{M}, \qquad \frac{1}{\delta t}(\rho_K^{n+1} - \rho_K^n) + \operatorname{div}_K(\rho^n \boldsymbol{u}^n) = 0, \tag{5b}$$

$$\forall K \in \mathcal{M}, \qquad \frac{1}{\delta t}(\rho_K^{n+1} e_K^{n+1} - \rho_K^n e_K^n) + \operatorname{div}_K(\rho^n e^n \boldsymbol{u}^n) + p_K^n \operatorname{div}_K \boldsymbol{u}^n = S_K^n, \tag{5c}$$

$$\forall K \in \mathcal{M}, \qquad p_K^{n+1} = (\gamma - 1)\ \rho_K^{n+1}\ e_K^{n+1}, \tag{5d}$$

$$\forall 1 \leq i \leq d,\ \forall \sigma \in \mathcal{E}, \qquad \frac{1}{\delta t}(\rho_{D_\sigma}^{n+1} u_{i,\sigma}^{n+1} - \rho_{D_\sigma}^{n} u_{i,\sigma}^{n}) + \mathrm{div}_\sigma(\rho^n u_i^n \boldsymbol{u}^n) + (\eth_i p)_\sigma^{n+1} = 0. \tag{5e}$$

2.1. **Discrete mass balance (Eqn.** (5b)**)**

Let us first address the discretization of the mass balance equation (1a). The discrete mass balance (5b) is of finite volume type, and is set out on the primal cells, since the density unknowns are associated with these cells. The divergence term is thus obtained by defining primal numerical fluxes $F_{K,\sigma}^n$ for each time step t^n across each faces σ outward of a cell $K \in \mathcal{M}$ as

$$\forall \sigma = K|L \in \mathcal{E}_{\mathrm{int}}, \quad F_{K,\sigma}^n = |\sigma|\ \rho_\sigma^n \boldsymbol{u}_\sigma^n \cdot \boldsymbol{n}_{K,\sigma},$$

with $\boldsymbol{n}_{K,\sigma}$ the normal vector to the face σ outward K and ρ_σ^n a discretization of the density at the face. Several choices are possible for this approximation at the face, as the upwind one, that is given by:

$$\rho_\sigma^n = \begin{cases} \rho_K^n & \text{if } \boldsymbol{u}_\sigma^n \cdot \boldsymbol{n}_{K,\sigma} \geq 0, \\ \rho_L^n & \text{otherwise.} \end{cases}$$

More precise techniques can also be derived, as for instance the MUSCL method of [10]. The divergence term of the discrete mass balance equation (1b) then reads:

$$\mathrm{div}_K(\rho^n \boldsymbol{u}^n) = \frac{1}{|K|} \sum_{\sigma \in \mathcal{E}(K)} F_{K,\sigma}^n. \tag{6}$$

2.2. **Discrete internal energy balance (Eqn.** (5c)**)**

We now address the discrete internal energy equation (5c). The convection term reads

$$\mathrm{div}_K(\rho^n \boldsymbol{u}^n e^n) = \frac{1}{|K|} \sum_{\sigma \in \mathcal{E}(K)} F_{K,\sigma}^n e_\sigma^n,$$

where the value at a face $\sigma = K|L \in \mathcal{E}_{\mathrm{int}}$ of the internal energy may be once again obtained by the MUSCL approximation of [10], or by a simple upwind approximation, that is

$$e_\sigma^n = \begin{cases} e_K^n & \text{if } F_{K,\sigma}^n \geq 0, \\ e_L^n & \text{otherwise.} \end{cases}$$

The divergence term is derived in the same fashion as the divergence term of the mass balance equation, and is thus given by:

$$\mathrm{div}_K \boldsymbol{u}^n = \frac{1}{|K|} \sum_{\sigma \in \mathcal{E}(K)} \boldsymbol{u}_\sigma^n \cdot \boldsymbol{n}_{K,\sigma}.$$

Finally, the term S_K^n is a corrective term which is added to ensure a kinetic energy stability result; its definition depends on the convection operator of the discrete momentum equation, or rather the technique used for the definition of the velocity on the dual faces. We refer to [10, 13] for its exact definition and for more details on its construction.

The values of the unknowns at the time step $n = 0$ are given by an average of the initial data:

$$\text{For } 1 \leq i \leq d,\ \forall \sigma \in \mathcal{E}, \qquad u^0_{\sigma,i} = \frac{1}{|D_\sigma|} \int_{D_\sigma} (\boldsymbol{u}_0(x))_i dx, \tag{7}$$

where $\boldsymbol{u}_0$ is the initial data.

2.3. **Discrete momentum balance (Eqn.** (5e)**)**

We now turn to the discrete momentum balance equation (1b). The discrete derivative $(\eth_i p)^n_\sigma$ is built at each face $\sigma \in \mathcal{E}$ and for all component $1 \leq i \leq d$, and is given as follows:

$$\forall \sigma \in \mathcal{E}_{\text{int}}, \sigma = K|L, \qquad (\eth_i p)^n_\sigma = \frac{|\sigma|}{|D_\sigma|}(p_L - p_K)\boldsymbol{n}_{K,\sigma} \cdot \boldsymbol{e}^{(i)}, \tag{8}$$

where $\boldsymbol{e}^{(i)}$ is the i^{th} vector of the orthonormal basis of $\mathbb{R}^d$, and $\boldsymbol{n}_{K,\sigma}$ the normal vector to the face σ outward the cell K.

The discrete divergence operator $\text{div}_\sigma(\rho^n u^n_i \boldsymbol{u}^n)$ is of finite-volume type, and, since the discretization is staggered, relies on the dual mesh. It takes the general form:

$$\text{for } 1 \leq i \leq d, \forall \sigma \in \mathcal{E}, \qquad \text{div}_\sigma(\rho^n u^n_i \boldsymbol{u}^n) = \frac{1}{|D_\sigma|} \sum_{\epsilon \in \tilde{\mathcal{E}}(D_\sigma)} F^n_{\sigma,\epsilon}\ u^n_{i,\epsilon} \tag{9}$$

where $\rho^{n+1}_{D_\sigma}$ and $\rho^n_{D_\sigma}$ stand for a density associated to the dual cell D_σ at times t^{n+1} and t^n, and $F^n_{\sigma,\epsilon}$ is a mass flux leaving D_σ through the dual face ϵ at time t^n.

The expression of the velocity at the dual face, *i.e.*of the quantity $u^n_{i,\epsilon}$ for $\epsilon = \sigma|\sigma'$ in Equation (9) may be obtained thanks to an upwind method, that is :

$$\text{for } 1 \leq i \leq d, \qquad u^n_{i,\epsilon} = \left| \begin{array}{ll} u^n_{i,\sigma} & \text{if } F^n_{\sigma,\epsilon} \geq 0 \\ u^n_{i,\sigma'} & \text{otherwise,} \end{array} \right.$$

In order to enhance the accuracy of the scheme, one may also choose an algebraic MUSCL technique, we refer to [5] for details on such a procedure.

The derivation of the quantities $\rho^{n+1}_{D_\sigma}$, $\rho^n_{D_\sigma}$ and $F^n_{\sigma,\epsilon}$ is performed to ensure a finite volume mass balance over the dual cells:

$$\text{for } 1 \leq i \leq d,\ \forall \sigma \in \mathcal{E}, \qquad \frac{|D_\sigma|}{\delta t}\ (\rho^{n+1}_{D_\sigma} - \rho^n_{D_\sigma}) + \sum_{\epsilon \in \tilde{\mathcal{E}}(D_\sigma)} F^n_{\sigma,\epsilon} = 0. \tag{10}$$

For σ in $\mathcal{E}_{\text{int}}$ such that $\sigma = K|L$, the approximate densities on the dual cell D_σ are given (at any time level) by the following weighted average:

$$|D_\sigma|\ \rho_{D_\sigma} = \xi^\sigma_K |K|\ \rho_K + \xi^\sigma_L |L|\ \rho_L, \qquad \text{with } \xi^\sigma_K = \frac{|D_{K,\sigma}|}{|K|},\ K \in \mathcal{M},\ \sigma \in \mathcal{E}(K). \tag{11}$$

For a (half) diamond cell associated to an external face, the density is equal to the density in the adjacent primal cell. Indeed, this identity is necessary to ensure a discrete kinetic energy balance, and the existence of a such balance equation is central to obtain consistent schemes (see [11–13]). The construction of the dual fluxes $F^n_{\sigma,\epsilon}$ for different grid cells is the subject of the next section.

3. Construction of the dual fluxes from the primal fluxes

In the following, we drop the time exponent for clarity. We first recall the conditions that must satisfy the set of dual fluxes $(F_{\sigma,\epsilon})_{\epsilon\subset K}$, is computed by solving a linear system depending on the primal fluxes $(F_{K,\sigma})_{\sigma\in\mathcal{E}(K)}$ appearing in the discrete mass balance, in order to obtain the stability of the resulting non linear convection operator.

Definition 3.1 (Constraints of the dual fluxes [1])**.** The fluxes through the faces of the dual mesh are defined so as to satisfy the following three constraints:

(H1) The discrete mass balance over the half-diamond cells is satisfied, in the following sense. For any primal cell K in $\mathcal{M}$, the set $(F_{\sigma,\epsilon})_{\epsilon\subset K}$ of dual fluxes included in K solves the following linear system

$$F_{K,\sigma} + \sum_{\epsilon\in\tilde{\mathcal{E}}(D_\sigma),\ \epsilon\subset K} F_{\sigma,\epsilon} = \xi_K^\sigma \sum_{\sigma'\in\mathcal{E}(K)} F_{K,\sigma'}, \qquad \sigma\in\mathcal{E}(K). \tag{12}$$

(H2) The dual fluxes are conservative, *i.e.* for any dual face $\epsilon = D_\sigma|D'_\sigma$, we have $F_{\sigma,\epsilon} = -F_{\sigma',\epsilon}$.

(H3) The dual fluxes are bounded with respect to the primal fluxes $(F_{K,\sigma})_{\sigma\in\mathcal{E}(K)}$ in the sense that there exists a universal constant real number C such that:

$$|F_{\sigma,\epsilon}| \le C\ \max\left\{|F_{K,\sigma}|, \qquad \sigma\in\mathcal{E}(K)\right\}, K\in\mathcal{M},\ \sigma\in\mathcal{E}(K),\ \epsilon\in\tilde{\mathcal{E}}(D_\sigma),\ \epsilon\subset K. \tag{13}$$

The assumptions (H1)-(H3) are sufficient to imply the consistency of the discrete convection operator, as we shall see later on. Note however that the system of equations (12) is singular and has an infinite number of solutions; the additional constraint (13) is needed for stability purposes, but the system (12)-(13) remains underdetermined. The choice of a particular solution to this system depends on the type of grid cell; it is detailed in the next paragraphs. Note that, since (12) is a linear system for the dual mass fluxes, a solution of (12) may be expressed as:

$$F_{\sigma,\epsilon} = \sum_{\sigma'\in\mathcal{E}(K)} \alpha_K^\epsilon F_{K,\sigma'}, \qquad \sigma\in\mathcal{E}(K),\ \epsilon\in\tilde{\mathcal{E}}(D_\sigma) \text{ and } \epsilon\subset K, \tag{14}$$

and the constraint (13) amounts to requiring the coefficients $(\alpha_K^\epsilon)_{\sigma,\sigma'\in\mathcal{E}(K)}$ to be bounded by a universal constant. In practice, the coefficients used in our numerical experimentations and derived below satisfy $|\alpha_K^\epsilon| \le 1$ for all $\sigma,\sigma'\in\mathcal{E}(K)$ and for all $K\in\mathcal{M}$.

We are thus able to cope with a quite general definition of the diamond cells, since, up to now, their volume itself is not specified. As mentioned in Section 1, in order to simplify the implementation, we however choose in practice to impose that the half-diamond cells of a primal cell K all have the same measure:

$$|D_{K,\sigma}| = |K|/\mathrm{card}(\mathcal{E}(K)). \tag{15}$$

Therefore, the real number ξ_K^σ in (11) and (12) takes the following values:

$$\xi_K^\sigma = \begin{cases} 1/3 \text{ for 2D simplices,} \\ 1/4 \text{ for 2D quadrangles and 3D simplices,} \\ 1/5 \text{ for quadrangle-based pyramids and triangular prisms,} \\ 1/6 \text{ for hexahedra,} \end{cases}$$

As a consequence, the system (12) only depends on the shape of the cell K under consideration. We may thus consider a particular geometry for K, and find an expression for the coefficients $((\alpha_K^\epsilon)_{\sigma,\sigma'\in\mathcal{E}(K)}$ which we apply to all similar cells, thus automatically satisfying the constraint (13).

3.1. **The case of a geometric dual mesh**

We first consider the case when the dual cells satisfying (15) can be geometrically built on a cell K in the sense that an explicit definition of $D_{K,\sigma}$ can be given for all $\sigma \in \mathcal{E}(K)$. This is for instance the case when K is a simplex, a square or a cube. Let us consider a momentum field $\boldsymbol{w}$ with constant divergence, such that:

$$\int_\sigma \boldsymbol{w}\cdot\boldsymbol{n}_{K,\sigma}\,\mathrm{d}\gamma(\boldsymbol{x}) = F_{K,\sigma}, \qquad \forall\sigma\in\mathcal{E}(K).$$

Then an easy computation shows that the definition

$$F_{\sigma,\epsilon} = \int_\epsilon \boldsymbol{w}\cdot\boldsymbol{n}_{\sigma,\epsilon}\,\mathrm{d}\gamma(\boldsymbol{x}), \tag{16}$$

where the unit vector normal to ϵ outward D_σ is denoted by $\boldsymbol{n}_{\sigma,\epsilon}$, satisfies (12) (see [1, Lemma 3.2]).

For instance, suppose that K is the reference square $K=[0,1]^2$. Next, denote by W, E, S, N the primal faces of K and F_W, F_E, F_S and F_N their associated primal fluxes, as in Figure 4. Then, it might be possible to choose the momentum field $\boldsymbol{w}$ as:

$$\boldsymbol{w}(x,y) = \begin{bmatrix}(1-x)(-F_W)+xF_E\\(1-y)(-F_S)+yF_N\end{bmatrix},$$

Next, we need to examine the connectivity inside the cell K. More precisely, for a given interface σ of K, $\sigma\in\{W,E,S,N\}$, we first list all the interfaces $\sigma'\in\{W,E,S,N\}\backslash\{\sigma\}$ such that $D_{K,\sigma}$ and $D_{K,\sigma'}$ are neighbouring dual cells. Let us denote by $F_{\sigma,\epsilon}$ denote the dual flux coming from the diamond cell $D_{K,\sigma}$ towards the diamond cell $D_{K,\sigma'}$ with $\epsilon=\sigma|\sigma'$. For each $\sigma\in\mathcal{E},\epsilon\in\tilde{\mathcal{E}}(D_\sigma),\epsilon\subset K$, we then obtain thanks to (16):

$$F_{\sigma,\epsilon} = \alpha_W^\epsilon F_W + \alpha_E^\epsilon F_E + \alpha_S^\epsilon F_S + \alpha_N^\epsilon F_N.$$

The set of coefficients $\{\alpha_K^\epsilon, \epsilon=\sigma|\sigma' \text{ with } \sigma,\sigma'\in\mathcal{E}(K)\}$ obtained in each case is given on Figure 4. The coefficients for simplicial cells are given on Fig. 2 and Fig. 3, and the coefficient for hexahedral cells are given on Tab. 3.1.

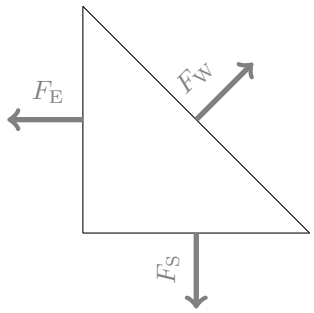

$\epsilon=\sigma\|\sigma'$	α_W^ϵ	α_E^ϵ	α_S^ϵ
$W\|S$	$-1/3$	0	$1/3$
$S\|E$	0	$1/3$	$-1/3$
$E\|W$	$1/3$	$-1/3$	0

$$F_{\sigma,\epsilon} = \alpha_W^\epsilon F_W + \alpha_E^\epsilon F_E + \alpha_S^\epsilon F_S + \\ + \alpha_N^\epsilon F_N.$$

FIGURE 2. Primal flux over a triangular cell and coefficient of the dual fluxes

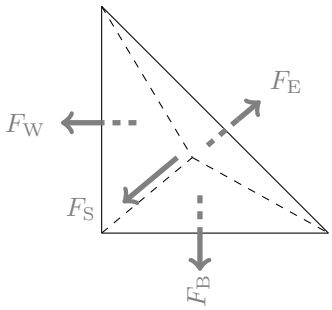

$\epsilon = \sigma\|\sigma'$	α^ϵ_W	α^ϵ_E	α^ϵ_S	α^ϵ_B
$B\|S$	0	0	1/4	−1/4
$B\|W$	1/4	0	0	−1/4
$B\|E$	0	1/4	0	−1/4
$S\|W$	1/4	0	−1/4	0
$W\|E$	− 1/4	1/4	0	0
$E\|S$	0	−1/4	1/4	0

$$F_{\sigma,\epsilon} = \alpha^\epsilon_W F_W + \alpha^\epsilon_E F_E + \alpha^\epsilon_S F_S + \alpha^\epsilon_N F_N + \alpha^\epsilon_B F_B$$

FIGURE 3. Primal flux over a tetrahedral cell and coefficient of the dual fluxes

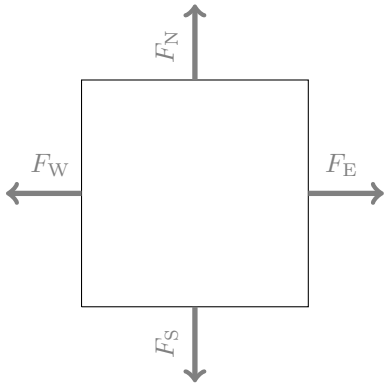

$\epsilon = \sigma\|\sigma'$	α^ϵ_W	α^ϵ_E	α^ϵ_S	α^ϵ_N
$W\|S$	− 3/8	1/8	3/8	−1/8
$S\|E$	− 1/8	3/8	−3/8	1/8
$E\|N$	1/8	−3/8	−1/8	3/8
$N\|W$	3/8	−1/8	1/8	−3/8

$$F_{\sigma,\epsilon} = \alpha^\epsilon_W F_W + \alpha^\epsilon_E F_E + \alpha^\epsilon_S F_S + \alpha^\epsilon_N F_N.$$

FIGURE 4. Primal flux over a quadrilateral cell and coefficient of the dual fluxes

3.2. **The case of a virtual dual mesh**

For highly distorted (*i.e.* far for parallelogram) quadrilaterals or hexahedra K of face σ, when the measure of σ is small with respect to the characteristic dimensions of K, it may be impossible to define $D_{K,\sigma}$ as a triangle or a pyramid, respectively, since such a volume of basis σ and included in K cannot satisfy $|D_{K,\sigma}| = |K|/\mathrm{card}(\mathcal{E}(K))$. In such a case, the similarity of the above-defined convection operator with a standard finite volume operator is only formal: indeed, its discrete formulation does not rely on the integration of the continuous operator over a control volume, whose shape and interfaces (and normal vectors) are not defined. For the same reasons, the method described in the above paragraph does not apply to prismatic and pyramidal cells. We thus present an algebraic technique to deal with those kinds of cells.

Let us suppose that K is a prismatic cell : we give a constructive process to deduce the dual fluxes directly from the system (12)-(13). Recall that a solution is not unique since the system is underdetermined, but it is still possible to deduce at least one solution. To fix ideas, we consider a prism with a triangular basis and denote by S, E, N, W and B the faces of the prism, so that F_S, F_E, F_N, F_W and F_B are the primal fluxes over the faces of the prism, as can be seen on Figure 3.2.

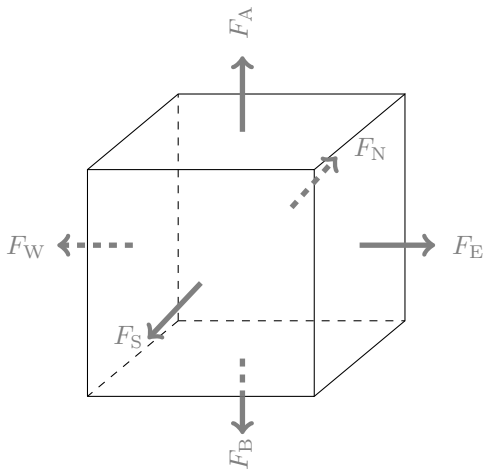

FIGURE 5. Primal flux over a hexahedral cell

$\epsilon = \sigma\|\sigma'$	α^ϵ_W	α^ϵ_E	α^ϵ_S	α^ϵ_N	α^ϵ_A	α^ϵ_B
$B\|S$	0	0	5/24	−1/24	1/24	−5/24
$S\|A$	0	0	−5/24	1/24	5/24	−1/24
$A\|N$	0	0	−1/24	5/24	−5/24	1/24
$N\|B$	0	0	1/24	−5/24	−1/24	5/24
$W\|S$	− 5/24	1/24	5/24	−1/24	0	0
$S\|E$	− 1/24	5/24	−5/24	1/24	0	0
$E\|N$	1/24	−5/24	−1/24	5/24	0	0
$N\|W$	5/24	−1/24	1/24	−5/24	0	0
$B\|E$	− 1/24	5/24	0	0	1/24	−5/24
$E\|A$	1/24	−5/24	0	0	5/24	−1/24
$A\|W$	5/24	−1/24	0	0	−5/24	1/24
$W\|B$	− 5/24	1/24	0	0	−1/24	5/24

$$F_{\sigma,\epsilon} = \alpha^\epsilon_W F_W + \alpha^\epsilon_E F_E + \alpha^\epsilon_S F_S + \alpha^\epsilon_N F_N + \alpha^\epsilon_A F_A + \alpha^\epsilon_B F_B.$$

TABLE 1. Coefficient of the dual fluxes for a hexahedral cell

Then, we denote once again for $\sigma, \sigma' \in \{D, S, E, N, W\}^2, \sigma \neq \sigma'$ by $F_{\sigma,\sigma'}$ the dual flux coming from the diamond cell associated with the face σ towards the diamond cell associated with the face σ', accordingly to the connectivity of the cell. Using the conservativity of the dual flux (that is $F_{\sigma,\epsilon} = -F_{\sigma',\epsilon}$), the system 12 may be written for the prism as:

$$AF_d = BF_p \tag{17}$$

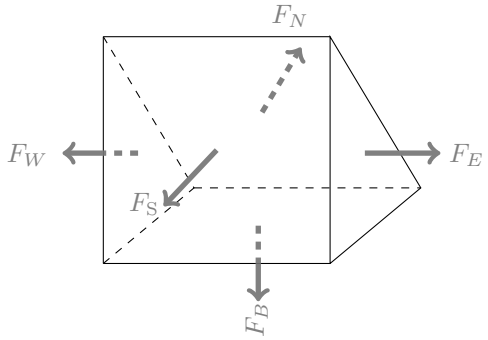

FIGURE 6. Primal fluxes over a prism

$\epsilon = \sigma\|\sigma'$	α_B^ϵ	α_S^ϵ	α_N^ϵ	α_E^ϵ	α_W^ϵ
$S\|N$	0	-1/5	1/5	0	0
$N\|B$	1/5	0	-1/5	0	0
$B\|S$	-1/5	1/5	0	0	0
$E\|B$	1/5	0	0	-4/15	1/15
$E\|S$	0	1/5	0	-4/15	1/15
$E\|N$	0	0	1/5	-4/15	1/15
$W\|B$	1/5	0	0	1/15	-4/15
$W\|S$	0	1/5	0	1/15	-4/15
$W\|N$	0	0	1/5	1/15	-4/15

$$F_{\sigma,\epsilon} = \alpha_W^\epsilon F_W + \alpha_E^\epsilon F_E + \alpha_S^\epsilon F_S + \alpha_N^\epsilon F_N + \alpha_B^\epsilon F_B.$$

TABLE 2. Coefficient of the dual fluxes for a prism

with

$$F_p = (F_U, F_S, F_N, F_E, F_W)^t,$$
$$F_d = (F_{S|N}, F_{N|U}, F_{U|S}, F_{E|U}, F_{E|S}, F_{E|N}, F_{W|U}, F_{W|S}, F_{W|N})^t,$$

where $F_{\sigma|\sigma'}$ denotes the dual flux coming from the diamond cell D_σ towards the diamond cell $D_{\sigma'}$ associated with the face σ', and

$$A = \begin{pmatrix} 0 & -1 & 1 & -1 & 0 & 0 & -1 & 0 & 0 \\ 1 & 0 & -1 & 0 & -1 & 0 & 0 & -1 & 0 \\ -1 & 1 & 0 & 0 & 0 & -1 & 0 & 0 & -1 \\ 0 & 0 & 0 & 1 & 1 & 1 & 0 & 0 & 0 \\ 0 & 0 & 0 & 0 & 0 & 0 & 1 & 1 & 1 \end{pmatrix},$$

$$B = \begin{pmatrix} -4/5 & 1/5 & 1/5 & 1/5 & 1/5 \\ 1/5 & -4/5 & 1/5 & 1/5 & 1/5 \\ 1/5 & 1/5 & -4/5 & 1/5 & 1/5 \\ 1/5 & 1/5 & 1/5 & -4/5 & 1/5 \\ 1/5 & 1/5 & 1/5 & 1/5 & -4/5 \end{pmatrix}.$$

Since the dual fluxes are supposed to be a linear combination of the primal fluxes, the vector F_d may be expressed as $F_d = XF_p$, where X is a matrix whose entries are the desired coefficients $\{\alpha^\epsilon_\sigma, \sigma \in \mathcal{E}(K), \epsilon = \sigma|\epsilon, \epsilon \in \mathcal{E}(K), \epsilon \neq \sigma\}$. Substituting this expression in (17), one obtains an underdetermined system $AX = B$, for which a solution are obtained through the least-square method. The coefficients thus obtained are given in the Figure 3.2.

The same technique is applied for a pyramidal mesh. The notation for its faces and its primal flux is the same as before, as can be seen in Figure 7. Note that the connectivity of the pyramid is similar to the one of the prism, up to the fact that the northern and southern dual cells are not connected. The linear system for a pyramidal mesh may thus be deduced from the prism one by removing any instance of the dual flux $F_{S|N}$. The coefficients are given in Table 7.

Note that the algebraic / least-square technique that we described for general cells may also be applied to the cells for which a geometrical construction is possible; we checked that the coefficients obtained through this technique are the same as those obtained by choosing the momentum field as in Section 3.1 and [1].

4. Lax-Wendroff consistency of the convection operator

The derivation of the discrete convection operator presented in the above section is based on stability arguments only; besides, neither the dual mass fluxes nor the shape of the dual control volumes themselves seem to be precisely defined, so that the method itself may appear rather puzzling. It then seems worth assessing its convergence properties.

Let us first mention that recent theoretical results have been already obtained for the type of scheme under study: in [14], the convection term of the variable density incompressible Navier-Stokes equations is discretized on quadrangles with the above method, and convergence of the approximate solutions is proven; in [2], a linearized version of this operator is shown to satisfy first-order error estimates. Last but not least, numerical experiments show that this discretization is in most tests more accurate than standard variants, see e.g. [10, 13]. Since we are dealing with the full Euler equations, we do not have enough estimates to ensure the compactness of the approximate solutions, and therefore we only show here the Lax-Wendroff consistency of this operator, that is to say, assuming some bounds and compactness on the sequence of approximate functions associated to a vanishing time and mesh steps, we prove that the weak form of the discrete convection operator tends to the weak form of the continuous convection operator. The proof relies on some general results [8, 9] which we recall in the appendix.

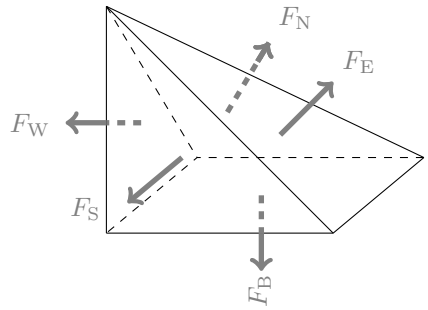

$\epsilon = \sigma\|\sigma'$	α_B^ϵ	α_S^ϵ	α_E^ϵ	α_N^ϵ	α_W^ϵ
$B\|S$	-1/5	4/15	0	-1/15	0
$B\|E$	-1/5	0	4/15	0	-1/15
$B\|N$	-1/5	-1/15	0	4/15	0
$B\|W$	-1/5	0	-1/15	0	4/15
$S\|E$	0	-4/15	4/15	1/15	-1/15
$E\|N$	0	-1/15	-4/15	4/15	1/15
$N\|W$	0	1/15	-1/15	-4/15	4/15
$W\|S$	0	4/15	1/15	-1/15	-4/15

$$F_{\sigma,\epsilon} = \alpha_W^\epsilon F_W + \alpha_E^\epsilon F_E + \alpha_S^\epsilon F_S + \alpha_N^\epsilon F_N + \alpha_B^\epsilon F_B.$$

FIGURE 7. Primal flux over a pyramidal cell and coefficient of the dual fluxes

Let $\mathcal{M}$ be a given mesh and let $\mathcal{T} = \{(t_n)_{n\in[\![0,N]\!]},\ t_n = n\,\delta t\}$ be a given time discretization of time step δt. We define the discrete function associated to the density and the velocity by:

$$\begin{aligned} &\rho(\boldsymbol{x},t) = \rho_K^{n+1} \text{ for } \boldsymbol{x}\in K,\ t\in(t_n,t_{n+1}],\ K\in\mathcal{M},\ n\in[\![0,N-1]\!],\\ &\boldsymbol{u}(\boldsymbol{x},t) = \boldsymbol{u}_\sigma^{n+1} \text{ for } \boldsymbol{x}\in D_\sigma,\ t\in(t_n,t_{n+1}],\ \sigma\in\mathcal{E},\ n\in[\![0,N-1]\!], \end{aligned} \tag{18}$$

and the interpolate of a test function φ by

$$\mathfrak{I}^{(m)}(\varphi)(\boldsymbol{x},t) = \varphi_\sigma^n \text{ for } \boldsymbol{x}\in D_\sigma \text{ and } t\in(t_n,t_{n+1}),$$
$$\text{with } \varphi_\sigma^n = \frac{1}{|D_\sigma|}\int_{D_\sigma}\varphi(\boldsymbol{x},t_n)\,\mathrm{d}\boldsymbol{x} \quad \text{for } \sigma\in\mathcal{E} \text{ and } n\in[\![0,N-1]\!]. \tag{19}$$

In the sequel, we also use the notation φ_K^n defined by:

$$\varphi_K^n = \frac{1}{|K|}\int_K \varphi(\boldsymbol{x},t_n)\,\mathrm{d}\boldsymbol{x} \qquad \text{for } K\in\mathcal{M} \text{ and } n\in[\![0,N-1]\!]. \tag{20}$$

The regularity of a mesh $\mathcal{M}$ is measured by the parameters $\theta_1(\mathcal{M})$ and $\theta_2(\mathcal{M})$ defined by

$$\theta_1(\mathcal{M}) = \max_{K\in\mathcal{M}} \frac{\mathrm{diam}(K)^d}{|K|}, \tag{21a}$$

$$\theta_2(\mathcal{M}) = \max\{\frac{|K|}{|L|},\ K \text{ and } L \text{ adjacent cells of } \mathcal{M}\}. \tag{21b}$$

For $i \in [\![1, d]\!]$, consider the (scalar) convection operator defined by:

$$\begin{aligned} \mathcal{C}_i(\rho, \boldsymbol{u}) :\quad & \Omega \times (0,T) \to \mathbb{R}, \\ & (\boldsymbol{x}, t) \mapsto \mathcal{C}^n_{i,\sigma}(\rho, \boldsymbol{u})_\sigma, \text{ for } \begin{cases} \boldsymbol{x} \in D_\sigma,\ \sigma \in \mathcal{E}, \\ t \in (t_n, t_{n+1}),\ n \in [\![0, N-1]\!], \end{cases} \end{aligned} \tag{22}$$

where, for $\sigma \in \mathcal{E}$ and $n \in [\![0, N-1]\!]$,

$$\mathcal{C}^n_{i,\sigma}(\rho, \boldsymbol{u})_\sigma = \frac{1}{\delta t}(\rho^{n+1}_{D_\sigma} u^{n+1}_{i,\sigma} - \rho^n_{D_\sigma} u^n_{i,\sigma}) + \mathrm{div}_\sigma(\rho^n u^n_i \boldsymbol{u}^n), \tag{23}$$

with $\mathrm{div}_\sigma(\rho^n u^n_i \boldsymbol{u}^n)$ defined by (9).

Theorem 4.1 (Lax-Wendroff consistency of the convection operator)**.** *Let $(\mathcal{M}^{(m)})_{m\in\mathbb{N}}$ and $(\mathcal{T}^{(m)})_{m\in\mathbb{N}}$ be a sequence of space-time discretisations be given, with $h_{\mathcal{M}^{(m)}}$ and $\delta t^{(m)}$ tending to zero, and let $(\rho^{(m)}, \boldsymbol{u}^{(m)})_{m\in\mathbb{N}}$ be an associated sequence of discrete functions. We suppose that*

$$\exists\ \theta \in \mathbb{R} \text{ such that } \max\{\theta_1(\mathcal{M}^{(m)}),\ \theta_2(\mathcal{M}^{(m)}),\ m \in \mathbb{N}\} \le \theta, \tag{24}$$

$$\exists\ N_{\mathcal{E}} \in \mathbb{R} \text{ such that } \max\{\mathrm{card}(\mathcal{E}(K)),\ K \in \mathcal{M}^{(m)},\ m \in \mathbb{N}\} \le N_{\mathcal{E}}. \tag{25}$$

We also suppose that there exist $C_1, C_2 \in \mathbb{R}_+$ independent of m, and that there exist $\bar\rho \in L^\infty(\Omega \times [0,T))$ and $\bar{\boldsymbol{u}} \in L^\infty(\Omega \times (0,T))^d$, such that

$$\|\rho^{(m)}\|_{L^\infty(\Omega\times(0,T))} \le C_1\ \forall m \in \mathbb{N}, \tag{26}$$

$$\|\boldsymbol{u}^{(m)}\|_{L^\infty(\Omega\times(0,T))^d} \le C_2\ \forall m \in \mathbb{N}, \tag{27}$$

$$\|\rho^{(m)} - \bar\rho\|_{L^\infty(\Omega\times(0,T))} \to 0 \text{ as } m \to +\infty, \tag{28}$$

$$\|\boldsymbol{u}^{(m)} - \bar{\boldsymbol{u}}\|_{L^\infty(\Omega\times(0,T))^d} \to 0 \text{ as } m \to +\infty. \tag{29}$$

For $i \in [\![,]\!]$, let $C^{(m)}_i(\rho^{(m)}, \boldsymbol{u}^{(m)})$ be the convection operator defined by (22)-(23) for each mesh $\mathcal{M}^{(m)}$. Then, for any function $\varphi \in C^\infty_c(\Omega \times (0,T))$,

$$\begin{aligned} \lim_{m\to+\infty} \int_0^T \int_\Omega \mathcal{C}^{(m)}_i(\rho^{(m)}, \boldsymbol{u}^{(m)})\ \mathcal{I}^{(m)}(\varphi)\,\mathrm{d}\boldsymbol{x}\,\mathrm{d}t \\ = -\int_\Omega \rho(\boldsymbol{x},0)\,u_i(\boldsymbol{x},0)\varphi(\boldsymbol{x},0)\,\mathrm{d}\boldsymbol{x} - \int_0^T \int_\Omega (\rho\,u_i\ \partial_t\varphi + \ \rho\,u_i\,\boldsymbol{u}\cdot\boldsymbol{\nabla}\varphi)\,\mathrm{d}\boldsymbol{x}\,\mathrm{d}t. \end{aligned} \tag{30}$$

Proof. Let $\varphi \in C_c^\infty(\Omega \times (0,T))$ be given. By definition of the convection operator, we have:

$$\int_0^T \int_\Omega \mathfrak{C}_i^{(m)}(\rho^{(m)}, \boldsymbol{u}^{(m)})\ \mathfrak{I}^{(m)}(\varphi)\,\mathrm{d}\boldsymbol{x}\,\mathrm{d}t = T^{(m)} + X^{(m)}$$

with

$$T^{(m)} = \sum_{n=0}^{N^{(m)}-1} \sum_{\sigma\in\mathcal{E}^{(m)}} |D_\sigma|\ \varphi_\sigma^n\ ((\rho^{(m)})_{D_\sigma}^{n+1}\ (u_i^{(m)})_\sigma^{n+1} - (\rho^{(m)})_{D_\sigma}^n\ (u_i^{(m)})_\sigma^n),$$
$$X^{(m)} = \sum_{n=0}^{N^{(m)}-1} \delta t^{(m)}\ (X^{(m)})^{n+1},$$

where

$$(X^{(m)})^n = \sum_{\sigma\in\mathcal{E}^{(m)}} \varphi_\sigma^n \sum_{\epsilon\in\tilde{\mathcal{E}}(D_\sigma)} F_{\sigma,\epsilon}^n(\rho^{(m)}, \boldsymbol{u}^{(m)})\ (u_i^{(m)})_\epsilon^n.$$

Throughout this proof, we suppose that the space and time steps are small enough for the test function φ to vanish in the boundary cells and at the last time step. Hence, "boundary terms" appear neither in time nor space discrete integration by parts.

The convergence of the time derivative term $T^{(m)}$ is obtained by applying [9, Lemma 2.7], which we recall in the appendix with weaker assumptions that are sufficient in the present work, see Lemma A.1. In this latter lemma, we choose $\mathfrak{P}^{(m)}$ to be the (virtual) dual mesh defined by the dual cells D_σ for $\sigma \in \mathcal{E}_{\rm int}$, and for each component of the velocity, $i = 1, \dots d$, the function β is defined by $\beta(\rho, u_i) = \rho u_i$; Let us first check that the condition (54) of Lemma A.1 is satisfied *i.e.* that

$$\sum_{\sigma\in\mathcal{E}_{\rm int}} \int_{D_\sigma} \left|(\rho^0 u_i^0)_{D_\sigma} - \rho_0(\boldsymbol{x}) u_{0,i}(\boldsymbol{x})\right|\,\mathrm{d}\boldsymbol{x} \to 0 \text{ as } m \to +\infty. \tag{31}$$

By (5a), $(\rho^0 u_i^0)_{D_\sigma} = \dfrac{1}{|D_\sigma|}\left(|D_{K,\sigma}|\rho_K^0 + |D_{L,\sigma}|\rho_L^0\right)(u_i^0)_\sigma$. Now, remark that

$$\frac{1}{|D_\sigma|}\left(|D_{K,\sigma}|\rho_0(\boldsymbol{x}) + |D_{L,\sigma}|\rho_0(\boldsymbol{x})\right) u_i^0(\boldsymbol{x}) = \rho_0(\boldsymbol{x}) u_{0,i}(\boldsymbol{x});$$

moreover the piecewise functions ρ^0 and u_i^0 defined by (5a) converge respectively to ρ_0 and $u_{0,i}$ in $L^p(0,T;\Omega)$ for any $p \geq 1$ so that the piecewise constant function $(\rho u_i)^0 = \sum_{\sigma\in\mathcal{E}_{\rm int}} (\rho^0 u_i^0)_{D_\sigma} \mathbb{1}_{D_\sigma}$ converges to $\rho_0 u_{0,i}$ in $L^p(0,T;\Omega)$ for any $p \in [1, +\infty[$. Therefore (31) holds.

Let us then show that the assumption (55) of Lemma A.1 holds; in the present context, it reads:

$$R_t^{(m)} = \sum_{n=0}^{N^{(m)}} \delta t^{(m)} \sum_{\substack{\sigma\in\mathcal{E}_{\rm int}^{(m)} \\ \sigma = K|L}} \int_{D_\sigma} |(\rho u_i)_{D_\sigma}^n - \rho^n(\boldsymbol{x}) u_i^n(\boldsymbol{x})|\,\mathrm{d}\boldsymbol{x} \to 0 \text{ as } m \to +\infty. \tag{32}$$

By the definition (11) of $\rho^n_{D_\sigma}$, we get that

$$R_t^{(m)} = \sum_{n=0}^{N^{(m)}} \delta t^{(m)} \sum_{\substack{\sigma \in \mathcal{E}_{\rm int}^{(m)} \\ \sigma = K|L}} I_\sigma$$

with

$$I_\sigma = \int_{D_\sigma} |(\frac{1}{|D_\sigma|}\left(|D_{K,\sigma}|\rho_K + |D_{L,\sigma}|\rho_L\right) u^n_{i,\sigma} - \rho^n(\boldsymbol{x}) u_i^n(\boldsymbol{x})|\,\mathrm{d}\boldsymbol{x}.$$

Let us decompose $I_\sigma = I_{K,\sigma} + I_{L,\sigma}$ with

$$\begin{aligned} I_{K,\sigma} &= |D_{K,\sigma}||(\frac{1}{|D_\sigma|}\left(|D_{K,\sigma}|\rho^n_K + |D_{L,\sigma}|\rho^n_L\right) u^n_{i,\sigma} - \rho^n_K u^n_{i,\sigma}| \\ &= \frac{|D_{K,\sigma}|}{|D_\sigma|}|((|D_{K,\sigma}|\rho^n_K + |D_{L,\sigma}|\rho^n_L\right) u^n_{i,\sigma} - |D_\sigma|\rho^n_K u^n_{i,\sigma}| \\ &= \frac{|D_{K,\sigma}||D_{L,\sigma}|}{|D_\sigma|}|\rho^n_K - \rho^n_L| u^n_{i,\sigma}. \end{aligned}$$

From the bound 27, we thus get that

$$R_t^{(m)} \leq 2 \sum_{n=0}^{N^{(m)}} \delta t^{(m)} \sum_{\substack{\sigma \in \mathcal{E}_{\rm int}^{(m)} \\ \sigma = K|L}} \frac{|D_{K,\sigma}||D_{L,\sigma}|}{|D_\sigma|}|\rho^n_K - \rho^n_L|.$$

The convergence to zero of $R_t^{(m)}$ follows thanks to Theorem A.3. Indeed, taking $\mathcal{P} = \mathcal{M}^{(m)}$, $P = K$, $Q = L$, it is clear that $\theta_{\mathcal{P}} = \max_{\substack{\sigma \in \mathcal{E}_{\rm int}^{(m)} \\ \sigma = K|L}} \frac{|D_{K,\sigma}|}{|K|}\frac{|D_{L,\sigma}|}{|D_\sigma|} \leq 1$.

We have thus proven that the assumptions of Lemma A.1 hold, and so that:

$$\lim_{m \to +\infty} T^{(m)} = -\int_\Omega \rho(\boldsymbol{x},0)\, u_i(\boldsymbol{x},0)\varphi(\boldsymbol{x},0)\,\mathrm{d}\boldsymbol{x} - \int_0^T \int_\Omega \rho\, u_i\ \partial_t\varphi\,\mathrm{d}\boldsymbol{x}\,\mathrm{d}t. \tag{33}$$

Let us now turn to the convection term. The first step in the analysis of this term consists in writing it as the sum of a remainder and a second term involving only the primal mass fluxes instead of the dual ones. Dropping the dependency on m at the right hand-side and decomposing the sum yields:

$$\begin{aligned} (X^{(m)})^n &= \sum_{\sigma \in \mathcal{E}^{(m)}} \varphi^n_\sigma \sum_{\epsilon \in \tilde{\mathcal{E}}(D_\sigma)} F^n_{\sigma,\epsilon}\ u^n_{i,\epsilon} \\ &= \sum_{K \in \mathcal{M}^{(m)}} \sum_{\sigma \in \mathcal{E}(K)} \varphi^n_\sigma \sum_{\substack{\epsilon \in \tilde{\mathcal{E}}(D_\sigma), \\ \epsilon \subset K}} F^n_{\sigma,\epsilon}\ u^n_{i,\epsilon}. \end{aligned} \tag{34}$$

For $K \in \mathcal{M}$ and $\sigma \in \mathcal{E}(K)$, let us recast the mass balance over the half-diamond cells (12) as:

$$\sum_{\epsilon \in \tilde{\mathcal{E}}(D_\sigma),\ \epsilon \subset K} F^n_{\sigma,\epsilon} = -F^n_{K,\sigma} + \xi_K\ (\eth\rho)^n_K \qquad \text{with } (\eth\rho)^n_K = \sum_{\sigma' \in \mathcal{E}(K)} F_{K,\sigma'}. \tag{35}$$

We recall that the coefficient ξ_K does not depend on the face of K (hence the suppression of the index σ in the notation) and only depends on the geometry of K (so, for instance, for a two-dimensional mesh of quadrangles, $\xi_K = 1/4$ for all the cells of the mesh). We now remark that, thanks to this relation,

$$\sum_{K \in \mathcal{M}^{(m)}} \sum_{\sigma \in \mathcal{E}(K)} \varphi^n_\sigma u^n_{i,\sigma} \sum_{\substack{\epsilon \in \tilde{\mathcal{E}}(D_\sigma),\\ \epsilon \subset K}} F^n_{\sigma,\epsilon} = -\sum_{K \in \mathcal{M}^{(m)}} \sum_{\sigma \in \mathcal{E}(K)} \varphi^n_\sigma u^n_{i,\sigma} F^n_{K,\sigma} + \sum_{K \in \mathcal{M}^{(m)}} \xi_K\ (\eth\rho)^n_K \sum_{\sigma \in \mathcal{E}(K)} \varphi^n_\sigma u^n_{i,\sigma}.$$

By conservativity, the first sum at the right hand-side of this relation vanishes. Thanks to this equation, we recast Equation (34) as $(X^{(m)})^n = (X^{(m)}_1)^n + (X^{(m)}_2)^n$ with

$$\begin{aligned} (X^{(m)}_1)^n &= \sum_{K \in \mathcal{M}^{(m)}} \sum_{\sigma \in \mathcal{E}(K)} \varphi^n_\sigma \sum_{\substack{\epsilon \in \tilde{\mathcal{E}}(D_\sigma),\\ \epsilon \subset K}} F^n_{\sigma,\epsilon}\ (u^n_{i,\epsilon} - u^n_{i,\sigma}), \\ (X^{(m)}_2)^n &= \sum_{K \in \mathcal{M}^{(m)}} \xi_K\ (\eth\rho)^n_K \sum_{\sigma \in \mathcal{E}(K)} \varphi^n_\sigma u^n_{i,\sigma}. \end{aligned} \tag{36}$$

Let us now decompose $(X^{(m)}_1)^n$ as $(X^{(m)}_1)^n = (X^{(m)}_3)^n + (R^{(m)}_1)^n$ with

$$\begin{aligned} (X^{(m)}_3)^n &= \sum_{K \in \mathcal{M}^{(m)}} \varphi^n_K \sum_{\sigma \in \mathcal{E}(K)} \sum_{\substack{\epsilon \in \tilde{\mathcal{E}}(D_\sigma),\\ \epsilon \subset K}} F^n_{\sigma,\epsilon}\ (u^n_{i,\epsilon} - u^n_{i,\sigma}), \\ (R^{(m)}_1)^n &= \sum_{K \in \mathcal{M}^{(m)}} \sum_{\sigma \in \mathcal{E}(K)} (\varphi^n_\sigma - \varphi^n_K) \sum_{\substack{\epsilon \in \tilde{\mathcal{E}}(D_\sigma),\\ \epsilon \subset K}} F^n_{\sigma,\epsilon}\ (u^n_{i,\epsilon} - u^n_{i,\sigma}). \end{aligned} \tag{37}$$

Let us show that

$$\sum_{n=0}^{N^{(m)}-1} \delta t^{(m)} (R^{(m)}_1)^n \to 0 \text{ as } m \to +\infty. \tag{38}$$

Firstly, by the mean value theorem, there exists C_3 depending only on φ such that

$$|\varphi^n_\sigma - \varphi^n_K| \le C_3(\mathrm{diam}(K) + \mathrm{diam}(L)).$$

Secondly, thanks to the definition (21a), one has

$$\mathrm{diam}(L)^d \le \theta^{(m)}_1 |L| \le \theta^{(m)}_1 \theta^{(m)}_2 |K| \le \theta^{(m)}_1 \theta^{(m)}_2 \mathrm{diam}(K)^d,$$

so that, thanks to the regularity (24) of the mesh,

$$\mathrm{diam}(K) + \mathrm{diam}(L) \le (1 + \theta^{2/d}) \mathrm{diam}(K),$$

and therefore

$$|\varphi_\sigma^n - \varphi_K^n| \leq C_3(1+\theta^{2/d})\mathrm{diam}(K). \tag{39}$$

By the definition (14) of the dual flux and owing to the L^∞ estimates (26) and (27), the following bound holds:

$$F_{\sigma,\epsilon} = \sum_{\sigma' \in \mathcal{E}(K)} \alpha_K^\epsilon F_{K,\sigma'} \leq C_1 C_2 \mathrm{diam}(K)^{d-1}, \sigma \in \mathcal{E}(K),\ \epsilon \in \tilde{\mathcal{E}}(D_\sigma) \text{ and } \epsilon \subset K,$$

Thirdly, for $\epsilon = \sigma|\sigma'$, $u_{i,\epsilon}^n$ is a convex combination of $u_{i,\sigma}^n$ and $u_{i,\sigma'}^n$. These three arguments together yield:

$$\begin{aligned}|(R_1^{(m)})^n| &\leq C_1 C_2 C_3 (1+\theta^{2/d}) \sum_{K\in\mathcal{M}} \mathrm{diam}(K)^d \sum_{\sigma\in\mathcal{E}(K)} \sum_{\substack{\epsilon\in\tilde{\mathcal{E}}^{(m)},\epsilon\subset K\\ \epsilon=\sigma|\sigma'}} |\boldsymbol{u}_\sigma^n - \boldsymbol{u}_{\sigma'}^n| \\ &\leq 3 C_1 C_2 C_3 (1+\theta^{2/d}) \sum_{\substack{\epsilon\in\tilde{\mathcal{E}}^{(m)}\\ \epsilon=\sigma|\sigma'\subset K}} \mathrm{diam}(K)^d |\boldsymbol{u}_\sigma^n - \boldsymbol{u}_{\sigma'}^n|.\end{aligned}$$

The assertion (38) then follows from Theorem A.3 given in the appendix. Indeed, we consider for $\mathcal{P}$ the mesh which consists of the cells $P_\epsilon = D_{K,\sigma} \cup D_{K,\sigma'}, \epsilon = \sigma|\sigma'$ where $K \in \mathcal{M}$ is such that $\epsilon \subset K$. Then Theorem A.3 holds provided that $\omega_{\sigma,\sigma'} = \dfrac{\mathrm{diam}(K)^d}{|D_{K,\sigma}| + |D_{K,\sigma'}|}$ is bounded independently of m; this is indeed true, since, thanks to the assumptions (15), (24) and (25),

$$\frac{\mathrm{diam}(K)^d}{|D_{K,\sigma}| + |D_{K,\sigma'}|} = \mathrm{card}\mathcal{E}(K) \frac{\mathrm{diam}(K)^d}{2|K|} \leq \frac{\theta N_\mathcal{E}}{2}.$$

Developing the term $(X_3^{(m)})^n$, we obtain

$$(X_3^{(m)})^n = \sum_{K\in\mathcal{M}^{(m)}} \varphi_K^n \sum_{\sigma\in\mathcal{E}(K)} \sum_{\substack{\epsilon\in\tilde{\mathcal{E}}(D_\sigma),\\ \epsilon\subset K}} F_{\sigma,\epsilon}^n\ u_{i,\epsilon}^n - \sum_{K\in\mathcal{M}^{(m)}} \varphi_K^n \sum_{\sigma\in\mathcal{E}(K)} u_{i,\sigma}^n \sum_{\substack{\epsilon\in\tilde{\mathcal{E}}(D_\sigma),\\ \epsilon\subset K}} F_{\sigma,\epsilon}^n.$$

By conservativity, the first sum at the right hand-side vanishes. Using once again (35), we then obtain $(X_3^{(m)})^n = (\tilde{X}^{(m)})^n + (X_4^{(m)})^n$

$$\begin{aligned}(\tilde{X}^{(m)})^n &= \sum_{K\in\mathcal{M}^{(m)}} \varphi_K^n \sum_{\sigma\in\mathcal{E}(K)} F_{K,\sigma}^n u_{i,\sigma}^n, \\ (X_4^{(m)})^n &= -\sum_{K\in\mathcal{M}^{(m)}} \xi_K\ (\eth\rho)_K^n\ \varphi_K^n \sum_{\sigma\in\mathcal{E}(K)} u_{i,\sigma}^n.\end{aligned} \tag{40}$$

We gather $(X_4^{(m)})^n$ with $(X_2^{(m)})^n$ to obtain yet another remainder term:

$$(R_2^{(m)})^n = (X_2^{(m)})^n + (X_4^{(m)})^n = \sum_{K\in\mathcal{M}^{(m)}} \xi_K\ (\eth\rho)_K^n \sum_{\sigma\in\mathcal{E}(K)} (\varphi_\sigma^n - \varphi_K^n)\ u_{i,\sigma}^n. \tag{41}$$

Let us show that $(R_2^{(m)})^n$ is indeed a remainder term, in the sense that

$$\sum_{n=0}^{N^{(m)}-1} \delta t^{(m)} (R_2^{(m)})^n \to 0 \text{ as } m \to +\infty. \tag{42}$$

For a given cell K, let $\boldsymbol{u}_K^n$ be the mean value of the velocities $\boldsymbol{u}_\sigma^n$ at the faces of K; since $\sum_{\sigma\in\mathcal{E}(K)} |\sigma|\ \rho_K^n\ \boldsymbol{u}_K^n \cdot \boldsymbol{n}_{K,\sigma} = 0$, we get

$$(\eth\rho)_K^n = \sum_{\sigma\in\mathcal{E}(K)} |\sigma|\ \rho_\sigma^n\ \boldsymbol{u}_\sigma^n \cdot \boldsymbol{n}_{K,\sigma} = \sum_{\sigma\in\mathcal{E}(K)} |\sigma|\ (\rho_\sigma^n\ \boldsymbol{u}_\sigma^n - \rho_K^n\ \boldsymbol{u}_K^n) \cdot \boldsymbol{n}_{K,\sigma}.$$

By the triangle inequality, owing to the the L^∞ estimates (26) and (27), using again (39), we get that there exists C_4 independent of m such that:

$$(R_2^{(m)})^n \le C_4(1+\theta^{2/d}) \sum_{K\in\mathcal{M}} \operatorname{diam}(K)^d \sum_{\sigma\in\mathcal{E}(K)} \left(|\rho_\sigma^n - \rho_K^n| + |\boldsymbol{u}_\sigma^n - \boldsymbol{u}_K^n|\right).$$

Since for $\sigma = K|L$, ρ_σ^n is a convex combination of ρ_K^n and ρ_L^n, and since $\boldsymbol{u}_K^n = \frac{1}{\operatorname{card}(\mathcal{E}(K))} \sum_{\sigma'\in\mathcal{E}(K)} \boldsymbol{u}_{\sigma'}^n$, we obtain:

$$(R_2^{(m)})^n \le C\theta(1+\theta^{2/d})[\sum_{\substack{\sigma\in\mathcal{E}_{\rm int}\\ \sigma=K|L}} (|K|+|L|)|\rho_K^n - \rho_L^n| + \sum_{\sigma\in\mathcal{E}_{\rm int}} |D_\sigma| \sum_{\substack{\epsilon\in\tilde{\mathcal{E}}^{(m)}\\ \epsilon=\sigma|\sigma'}} |\boldsymbol{u}_\sigma^n - \boldsymbol{u}_{\sigma'}^n|].$$

Invoking once again Theorem A.3 with the primal mesh $\mathcal{M}^{(m)}$ for the first sum of the right hand-side and the dual mesh for the second one, yields that (42) holds.

Let us finally prove the convergence of the term $(\tilde{X}^{(m)})^n$. This sum is the weak form of the divergence part of a new convection operator, posed on primal cells, and defined by:

$$\begin{aligned} \mathcal{C}_{\mathcal{M}}(\rho,\boldsymbol{u}): \quad & \Omega\times(0,T)\to\mathbb{R}, \\ & (\boldsymbol{x},t)\mapsto \mathcal{C}_K^n(\rho,\boldsymbol{u}), \text{ for } \begin{cases} \boldsymbol{x}\in K,\ K\in\mathcal{M}, \\ t\in(t_n,t_{n+1}),\ n\in[\![0,N-1]\!], \end{cases} \end{aligned}$$

where, for $K\in\mathcal{M}$ and $n\in[\![0,N-1]\!]$,

$$C_K^n(\rho,\boldsymbol{u}) = \sum_{\sigma\in\mathcal{E}(K)} F_{K,\sigma}^n\ u_{i,\sigma}^n.$$

Invoking Lemma A.2, we thus have to check the consistency of the flux defined by $G_{K,\sigma} = F_{K,\sigma}^n\ u_{i,\sigma}^n$ for $K\in\mathcal{M}$ and $\sigma\in\mathcal{E}(K)$, that is to say assumption (57). For $\boldsymbol{x}\in K$, the approximate density is $\rho(\boldsymbol{x}) = \rho_K$ and the approximate velocity $\boldsymbol{u} = \sum_{\sigma'\in\mathcal{E}(K)} \boldsymbol{u}_{\sigma'} \mathbb{1}_{D_{K,\sigma'}}$. Since $|K| = \operatorname{card}(\mathcal{E}(K))|D_{K,\sigma'}|$ for any $\sigma'\in\mathcal{E}(K)$, the left hand-side of assertion (57) reads, for the operator at hand:

$$R_{\rm div}^{(m)} = \sum_{n=0}^{N^{(m)}-1} \delta t^{(m)} \sum_{K\in\mathcal{M}^{(m)}} \operatorname{diam}(K) \sum_{\sigma\in\mathcal{E}_{\rm int}(K)} R_{K,\sigma}^n,$$

with

$$R^n_{K,\sigma} = |\sigma| \left| \boldsymbol{n}_{K,\sigma} \cdot \frac{1}{\mathrm{card}(\mathcal{E}(K))} \sum_{\sigma' \in \mathcal{E}(K)} \rho^n_\sigma \; u^n_{i,\sigma} \; \boldsymbol{u}^n_\sigma - \rho^n_K \; u^n_{i,\sigma'} \; \boldsymbol{u}^n_{\sigma'} \right|.$$

In this relation, ρ^n_σ stands for the approximation of the density at the face σ, and is a convex approximation of ρ^n_K and ρ^n_L where K and L are the cells separated by σ. The proof that $R^{(m)}_{\mathrm{div}}$ tends to zero relies on Theorem A.3. So, we have to recast this term as a collection of jumps, in time or in space, and show that the weights of these jumps are such that Theorem A.3 applies. By the triangle inequality and owing to the bounds (26) and (27), we obtain

$$R^n_{K,\sigma} \leq |\sigma| \; \left[C_2^2 |\rho^n_\sigma - \rho^n_K| + 2 C_2 C_1 |\boldsymbol{u}^n_\sigma \; - \boldsymbol{u}^n_{\sigma'}| \right] \tag{43}$$

Hence $R^{(m)}_{\mathrm{div}} \leq T^{(m)}_\rho + T^{(m)}_{\boldsymbol{u}}$ with

$$T^{(m)}_\rho \leq C_2^2 \sum_{n=0}^{N^{(m)}-1} \delta t^{(m)} \sum_{K \in \mathcal{M}^{(m)}} \mathrm{diam}(K) \sum_{\sigma \in \mathcal{E}_{\mathrm{int}}(K)} |\sigma| \; |\rho^n_\sigma - \rho^n_K| \tag{44}$$

$$T^{(m)}_{\boldsymbol{u}} \leq 2 C_2 C_1 \sum_{n=0}^{N^{(m)}-1} \delta t^{(m)} \sum_{K \in \mathcal{M}^{(m)}} \mathrm{diam}(K) \sum_{\sigma \in \mathcal{E}_{\mathrm{int}}(K)} |\sigma| |\boldsymbol{u}^n_\sigma \; - \boldsymbol{u}^n_{\sigma'}|. \tag{45}$$

Remarking that for $\sigma = K|L$, ρ^n_σ is a convex combination of ρ^n_K and ρ^n_L, it follows that

$$T^{(m)}_\rho \leq C_2^2 \sum_{n=0}^{N^{(m)}-1} \delta t^{(m)} \sum_{K \in \mathcal{M}^{(m)}} \mathrm{diam}(K) \sum_{\substack{\sigma \in \mathcal{E}_{\mathrm{int}}(K) \\ \sigma = K|L}} |\sigma| \; |\rho^n_K - \rho^n_L|,$$

so that, thanks to the regularity of the sequence of meshes,

$$T^{(m)}_\rho \leq C_2^2 \theta \sum_{n=0}^{N^{(m)}-1} \delta t^{(m)} \sum_{\sigma \in \mathcal{E}_{\mathrm{int}}, \; \sigma = K|L} (|K| + |L|) \; |\rho^n_K - \rho^n_L|,$$

which converges to zero thanks to Theorem A.3, still by regularity of the sequence of meshes.

Reordering the summation in the bound (45) of $T^{(m)}_{\boldsymbol{u}}$, we get that:

$$\begin{aligned} T^{(m)}_{\boldsymbol{u}} &\leq 2 C_2 C_1 \sum_{n=0}^{N^{(m)}-1} \delta t^{(m)} \sum_{K \in \mathcal{M}^{(m)}} \mathrm{diam}(K) \sum_{\sigma \in \mathcal{E}(K)} |\sigma| \sum_{\sigma' \in \mathcal{E}(K)} |\boldsymbol{u}^{n+1}_\sigma - \boldsymbol{u}^{n+1}_{\sigma'}| \\ &\leq 2 C_2 C_1 \sum_{n=0}^{N^{(m)}-1} \delta t^{(m)} \sum_{\substack{\epsilon \in \tilde{\mathcal{E}}^{(m)}, \; \epsilon \subset K, \\ \epsilon = \sigma|\sigma'}} \mathrm{diam}(K) \; (|\sigma| + |\sigma'|) \; |\boldsymbol{u}^{n+1}_\sigma - \boldsymbol{u}^{n+1}_{\sigma'}|, \end{aligned}$$

and the convergence to zero of $T_{\boldsymbol{u}}^{(m)}$ again follows by Theorem A.3, by construction of the dual cells, $|D_{K,\sigma}| = |D_{K,\sigma'}| = |K|/\mathrm{card}(\mathcal{E}(K))$ and since $\mathrm{diam}(K)\,(|\sigma| + |\sigma'|) \leq 2\,\theta\ |K|$. Hence

$$\lim_{m\to+\infty} (\tilde{X}^{(m)})^n = -\int_\Omega \rho(\boldsymbol{x},0)\, u_i(\boldsymbol{x},0)\varphi(\boldsymbol{x},0)\,\mathrm{d}\boldsymbol{x} - \int_0^T \int_\Omega (\rho\, u_i\ \partial_t\varphi +\ \rho\, u_i\, \boldsymbol{u}\cdot\boldsymbol{\nabla}\varphi)\,\mathrm{d}\boldsymbol{x}\,\mathrm{d}t.$$

This limit, together with the limits (38),(41), concludes the proof of Theorem 4.1. □

5. Numerical tests

In this section, we present numerical tests to assess the validity of the proposed discretization. The computations presented here are performed with the open-source CALIF^{3}S software developed at IRSN [6].

5.1. **A three dimensional Mach=10 shock on a column**

We consider here the problem of a uniform three-dimensional shock, that is impeded by an obstacle in the form of a circular column. Indeed, the domain Ω consists in the $[0, 0.4] \times [0, 0.41] \times [0, 0.4]$ cube, with a cylindrical column of radius 0.1 and height 0.3, which has the center of its basis located at the point $(0.2, 0.2, 0)$.

At the initial time, the flow is supposed at rest, and is initialized with the right state of the problem, that is:

$$\begin{bmatrix} \boldsymbol{u}_R = (0,0,0)^t \\ \rho_R = 1.4 \\ p_R = 1 \end{bmatrix}.$$

Then, a strong shock is supposed to be coming uniformly from the left side of the domain, with the given profile:

$$\begin{bmatrix} \boldsymbol{u}_L = (8.25,0,0)^t \\ \rho_L = 8 \\ p_L = 116.5 \end{bmatrix}.$$

This profile is determined through the Rankine-Hugoniot conditions, to retrieve a velocity of the shock equal to $\omega = 10$. Moreover, the coefficient γ is equal to $\gamma = 1.4$, so the speed of sound in the pre-shock state is equal to $c = \sqrt{\frac{\gamma p}{\rho}} = 1$ (which explains the Mach number $M = \omega/c = 10$).

The other boundaries condition are given as follows: outlet boundaries conditions are imposed on the right side of the domain, whereas all the other boundaries (that is the upper, lower, front and behind faces of the box, as well as the cylinder) are considered as walls with slip boundary conditions.

The problem is tested on prismatic and pyramidal meshes. The meshes are constructed as follows: first, a quadrilateral mesh of the bottom of the box is built so as to carefully fit the contour of the obstacle; it consists in 30160 quadrilaterals. A coarse version of this mesh, with and without the obstacle, can be seen in Figure 8. Then, if one wants a prismatic mesh, the quadrangles are split along a diagonal to obtain triangles. The resulting triangles are then extruded into 123 layers in the z-direction to form prismatic cells. The pyramidal mesh is obtained by extruding the quadrangles once again in 123 layers, thus leading to a hexahedra mesh; the hexahedra are then decomposed into six pyramids. Finally, the mesh is perforated to fit the cylindrical column. This leads to very fine meshes, composed of 6828960 cells for the prismatic mesh and 20486880 cells for the pyramidal one. A section of the coarse version of both meshes can be seen in Figure 9.

The results are given on Figure 10 and 11, in the form of sections of the domain at different heights: one at the bottom of the column, one just on top of the column and one at the top of the domain. On both meshes, the results

are similar. This has to be expected since both meshes are very refined, so the computation can be considered as converged. Moreover, the results are conforming to what can be expected. Indeed, at the top of the domain, the shock is not perturbed by the column, so the profile is identical to a pure shock problem. At the foot of the column, the shock bounces on the obstacle, which creates a zone with high density. This also causes the creation of a Mach stem on the right part of the obstacle. At the top of the column, the profile is as expected an intermediary step between the two previous profiles.

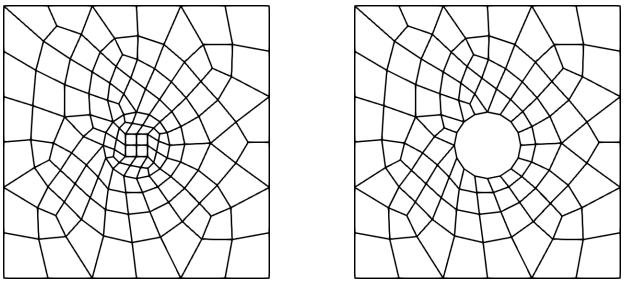

FIGURE 8. Two dimensional coarse mesh for the shock on a column

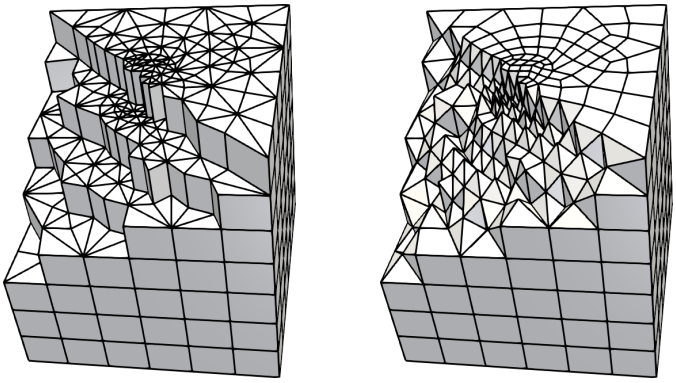

FIGURE 9. Cut on the above part of the three dimensional coarse meshes for the shock on a column. Left: prismatic mesh. Right: pyramidal mesh.

5.2. **A shock with reflexive boundary condition**

We finally turn to a test case where an analytical solution may be obtained through the Rankine-Hugoniot conditions. We first consider a one dimensional domain $\Omega_{1D} = [0, 5]$. At the initial time $t = 0$, and for all $x < 2$, the solution is supposed to be "at rest" in the left part of the domain, with a profile given by:

$$\begin{bmatrix} u_{L1} = 0 \\ \rho_{L1} = 1.292 \\ p_{L1} = 10^5 \end{bmatrix}, \tag{46}$$

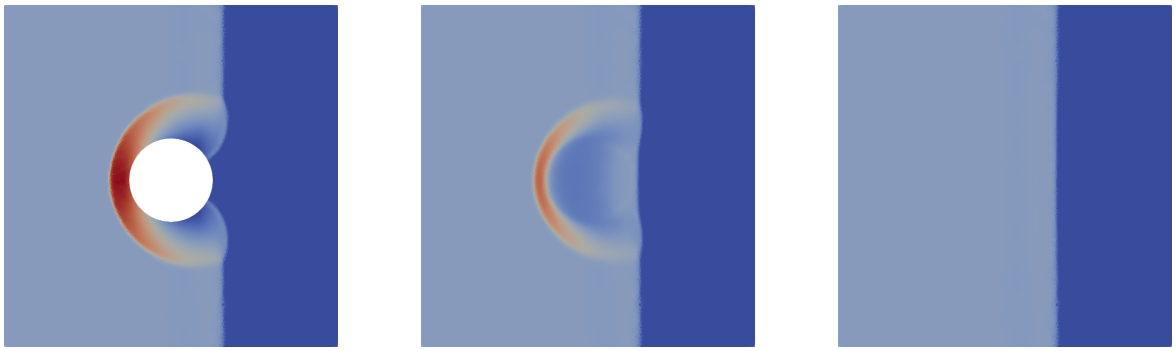

FIGURE 10. Density for the problem of the shock on a column on a prismatic mesh, at time $t = 0.026$. From left to right : cut at $z = 0.01$, cut at $z = 0.31$ and cut at $z = 0.4$.

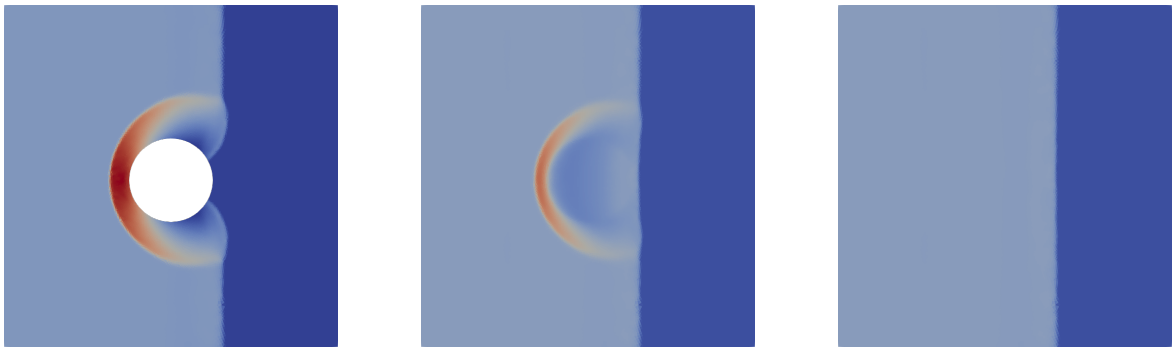

FIGURE 11. Density for the problem of the shock on a column on a pyramidal mesh, at time $t = 0.026$. From left to right : section at $z = 0.01$, $z = 0.31$ and $z = 0.4$.

We suppose that a shock is formed with a Mach number equal to $M = 10$. Since the Mach number is defined as $M = \frac{\omega}{c}$, where $c = \sqrt{\frac{\gamma p_{L1}}{\rho_{L1}}}$ is the speed of sound in the pre-shock state (and $\gamma = 1.4$) and ω is the velocity of the shock, we can determine the right part of the solution for $x \geq 2$, which is given by:

$$\begin{bmatrix} u_{R1} = 2c\frac{1-M^2}{M(1+\gamma)} \\ \rho_{R1} = \frac{M^2(1+\gamma)}{M^2(\gamma-1)+2}\rho_{L1} \\ p_{R1} = \frac{2\gamma M^2+1-\gamma}{1+\gamma}p_{L1} \end{bmatrix}, \tag{47}$$

The shock then moves from the right to the left; on the left side of the domain, reflexive boundary conditions are imposed, whereas Dirichlet boundary conditions are imposed on the right side of the domain, with the values being fixed by the right state.

For this problem, we can determine the exact solution up to a certain time T_{max}. Indeed, up to a time $T_{\text{sym}} = \frac{2}{\omega}$, the exact solution is given by the left state for $x < 2 - \omega t$ and by the right state for $x \geq 2 - \omega t$. At the time T_{sym}, the shock reflects on the left boundary. Due to the reflexive boundary conditions, another shock is obtained, for

which the velocity on the new left state u_{L2} is equal to zero, whereas the right state is given as previously, that is:

$$\begin{bmatrix} u_{R2} = u_{R1} \\ \rho_{R2} = \rho_{R1} \\ p_{R2} = p_{R1} \end{bmatrix}, \tag{48}$$

Using the Rankine-Hugoniot condition, one may determine ω_2 the velocity in the newly formed shocked, that is:

$$\omega_2 = u_{R1}\frac{3-\gamma}{4} + \frac{1}{2}\sqrt{\frac{(u_{R1}(\gamma+1))^2}{4} + 4\frac{\gamma p_{R1}}{\rho_{R1}}}$$

and the new left state, given by:

$$\begin{bmatrix} u_{L2} = 0 \\ \rho_{L2} = \frac{\rho_{R1}(\omega_2 - u_{R1})}{\omega_2} \\ p_{L2} = \rho_{R1}u_{R1}(u_{R1} - \omega_2) + p_{R1} \end{bmatrix}, \tag{49}$$

Then, for $t \in [T_{\text{sym}}, T_{max}]$, where T_{max} is the time at which the shock reaches the right boundary, *i.e.* $T_{\text{max}} = \frac{5}{\omega_2} + T_{\text{sym}}$, the solution is given by the left state $L2$ for $x < \omega_2(t - T_{\text{sym}})$ and by the right state $x \geq \omega_2(t - T_{\text{sym}})$.

To determine the accuracy of the scheme using three-dimensional cells, the domain Ω_{1D} is enhanced for the numerical tests into a three-dimensional domain, given by $\Omega = \Omega_{1D} \times [0, 10h] \times [0, 10h]$, where h is the space step into the x direction, equal to $h = \frac{5}{2^n}$ where n will be varying in order to built refined meshes. This choice of length and height of the domain is motivated by the fact that the solution should be independent of those two directions. It is possible to take a low amount of cells in these directions to reduce the number of unknowns, while still keeping the mesh step in these directions proportional to the mesh step in the x direction. The mesh is then built as follows:

- first, a 10×10 Cartesian grid of the y, z plan is built, using squares of side length equal to h ;
- then, a distortion is applied to this grid ;
- an extrusion in 2^n cells is then applied to the grid into the x direction, to retrieve the domain Ω_{1D} ;
- finally, the hexahedra obtained in the previous step are refined into either two prisms or two pyramids, depending on the kind of cell types wanted.

We also test this problem on a hybrid mesh, composed of hexahedral, pyramidal and prismatic cells. To do so, the considered domain is this time $\Omega' = \Omega_{1D} \times [0, 9h] \times [0, 9h]$. The mesh is constructed in the following way: first, three meshes of height $3h$ are build then glued together along the slices so as to completely mesh the domain Ω'. These meshes are constructed as previously, and are composed in order of hexahedra, pyramids and prisms. As a result, the global mesh is deformed, so that the layers of meshes are not stacked in a Cartesian way, but rather by forming layers closer to what can be found in practical cases of use of hybrid meshes. This transformation sends in particular $\partial\Omega$ over $\partial\Omega$, and is given by

$$T(x, y, z) = \begin{pmatrix} 1. + 0.2\sin(\frac{\pi x}{5})\sin(\frac{2\pi z}{9h})x \\ y \\ z \end{pmatrix} \tag{50}$$

The initial and boundary conditions are then prescribed as previously: the two last components of the velocity are set to zero. The analytical solution can be obtained in the same fashion. On the newly created boundary, wall boundary conditions of type slip are enforced.

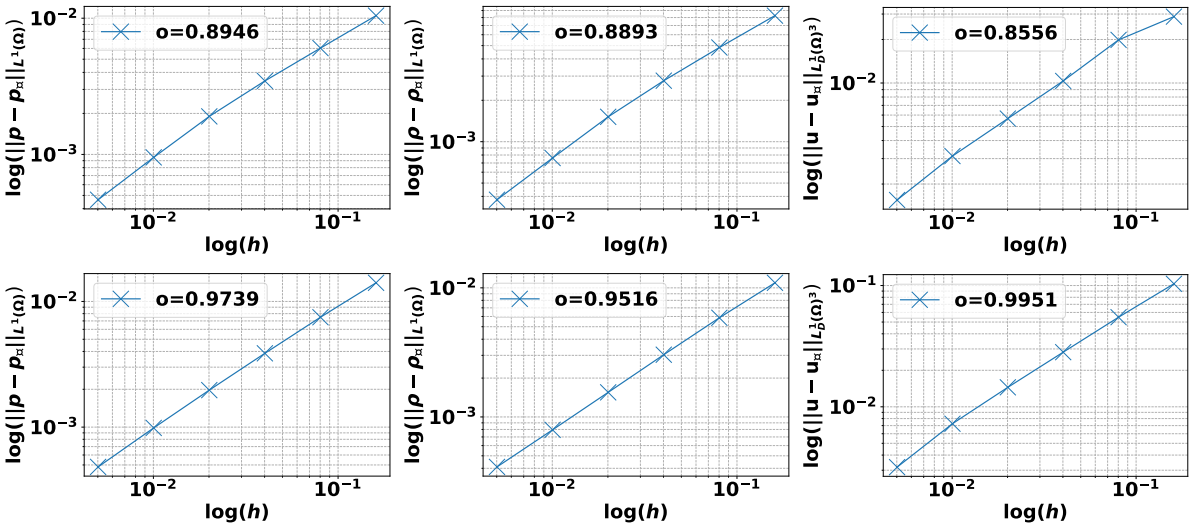

FIGURE 12. Convergence rate for the problem of a shock with reflexive boundary condition on a sequence of prismatic meshes. From left to right : pressure in $L^1(\Omega)$ norm, density in $L^1(\Omega)$ norm, velocity in discrete $L^1(\Omega)^d$ norm. From top to bottom : error at time $t = 0.003$, errors at time $t = 0.015$.

MUSCL approximations for both convection operators are chosen. A stabilization term is added to the discrete momentum balance equation, which is of the form:

$$\sum_{\substack{\epsilon \in \tilde{\mathcal{E}}(D_\sigma),\\ \epsilon = D_\sigma | D_{\sigma'}}} \nu_\epsilon^{n+1} (u_{\sigma,i}^n - u_{\sigma',i}^n)$$

where ν_ϵ is an user fixed parameter set to $\nu_\epsilon = \frac{|u_{R1}\rho_{R1}|}{50}$. The computation is ran until $T = 0.015$, which is slightly lower than T_{max}.

The convergence rate in $L^1(\Omega)$ for the pressure and the density, as well as the convergence rate in discrete $L^1(\Omega)^d$ norm for the velocity are computed at times $t_0 = 0.003$ (which is before the shock bounces on the left part of the domain) and $t_1 = 0.015$. The latter norm is computed by summing on each cell the volume of the cell multiplied by the value of the function at the gravity center of the cell. Moreover, we use in each case a relative norm, that is we divide the norm of the error by the norm of the exact solution over the whole domain. Indeed, since the length and height of the domain are scaled with the space step, the error norms (as well as the norm of the exact solution) are scaled with an additional factor proportional to h^2. By taking the relative norms, we ensure that the computed convergence rate is not impacted by this factor. The sequence of meshes is built by taking $n \in [\![6, 11]\!]$. The error curves for the different variables on prismatic meshes (resp. pyramidal, hybrid) can be found on Fig. 12 (resp. Fig. 13, Fig.14. These results are satisfying, since on both sequence of meshes and for all quantities a convergence rate close to 1 is recovered.

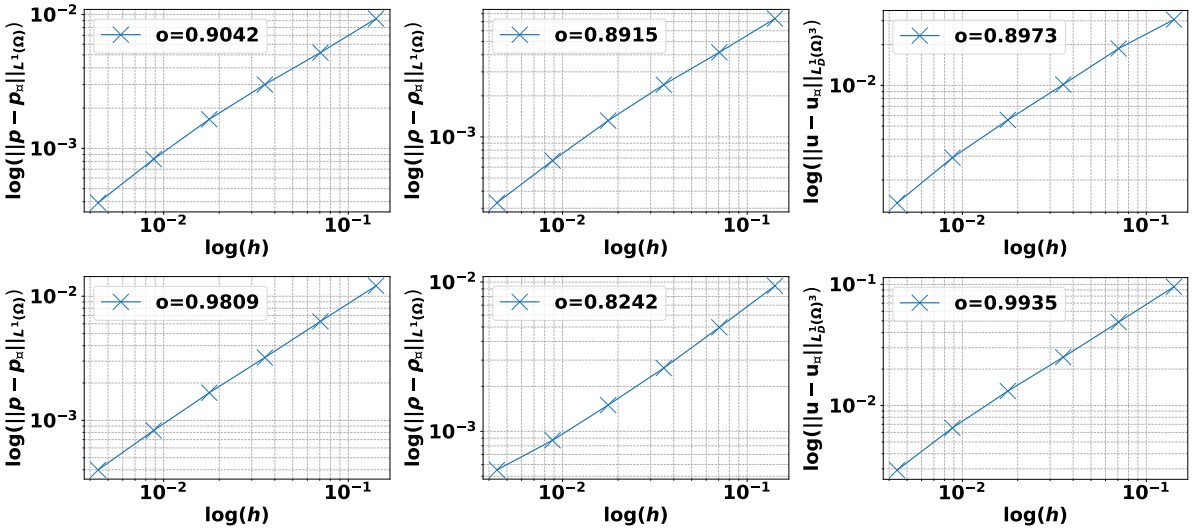

FIGURE 13. Convergence rate for the problem of a shock with reflexive boundary condition on a sequence of pyramidal meshes. From left to right : pressure in $L^1(\Omega)$ norm, density in $L^1(\Omega)$ norm, velocity in discrete $L^1(\Omega)^d$ norm. From top to bottom : error at time $t = 0.003$, errors at time $t = 0.015$.

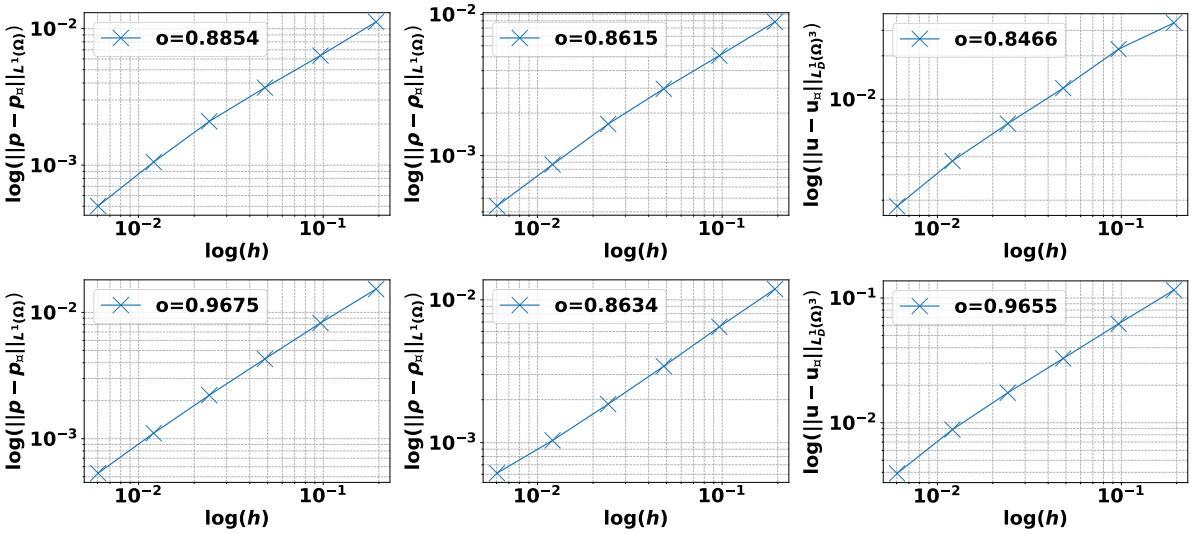

FIGURE 14. Convergence rate for the problem of a shock with reflexive boundary condition on a sequence of hybrid meshes. From left to right : pressure in $L^1(\Omega)$ norm, density in $L^1(\Omega)$ norm, velocity in discrete $L^1(\Omega)^d$ norm. From top to bottom : error at time $t = 0.003$, errors at time $t = 0.015$.

Appendix A. Technical lemmas

We recall here some results obtained in [8] and [9] which generalize the Lax-Wendroff consistency to multidimensional colocated or staggered grids.

We rephrase here the consistency results proven in [9], in a form that is adapted to the present setting. We suppose that:

$$\Omega \subset \mathbb{R}^d,\ d = 1, 2, 3,\ T \in (0, +\infty),\ p \in \mathbb{N}^*,\ \beta \in C^0(\mathbb{R}^p, \mathbb{R}),\ \boldsymbol{f} \in C^0(\mathbb{R}^p, \mathbb{R}^d), \tag{51}$$

and we consider the conservative convection operator $\bar{\mathcal{C}}(\bar{U})$ acting on a vector $\bar{U} \in \mathbb{R}^p$ of functions, real-valued, and defined (in the distributional sense), for $\bar{U} \in L^\infty(\Omega \times (0,T), \mathbb{R}^p)$, by:

$$\begin{aligned} \bar{\mathcal{C}}(\bar{U}):\quad & \Omega \times (0,T) \to \mathbb{R}, \\ & (\boldsymbol{x}, t) \mapsto \partial_t(\beta(\bar{U}(\boldsymbol{x}, t))) + \operatorname{div}(\boldsymbol{f}(\bar{U}(\boldsymbol{x}, t))). \end{aligned} \tag{52}$$

Let us denote by $(\mathcal{P}^{(m)})m \in \mathbb{N}$ a sequence of meshes of the domain Ω, each mesh consisting of a set of disjoint open polyhedral or polygonal open subsets of Ω, whose union of closures is $\bar{\Omega}$. We denote by $\delta(\mathcal{P})$ the space step, defined by

$$\delta(\mathcal{P}^{(m)}) = \max_{P \in \mathcal{P}^{(m)}} \operatorname{diam}(P).$$

Let $\mathfrak{F}^{(m)}$ denote the set of faces (in 3D, or edges in 2D) of the mesh, and $\mathfrak{F}^{(m)}_{\rm int}$ denote the set of faces that are not located on the boundary $\partial\Omega$; for a given polyhedron (or polygon) $P \in \mathcal{P}^{(m)}$, also called a cell, let $\mathfrak{F}(P)$ denote its set of faces (or edges). Let $\delta t^{(m)} = \frac{T}{N_m}$, with $N_m \in \mathbb{N}$, $\delta t^{(m)} \to 0$ as $m \to +\infty$, and let $t_n = n\delta t^{(m)}$ for $n \in [\![0, N_m]\!]$.

The unknown is supposed to be represented by a function $U \in L^\infty(\Omega \times (0,T), \mathbb{R}^p)$ (we take $U = (\rho, \boldsymbol{u})$ in Section 4). Note that the unknowns do not need to be piecewise-constant over the cells of the mesh and over the time steps.

The first result defines the weak consistency property, also referred to as consistency in the Lax-Wendroff sense, and provides a set of assumptions which are sufficient for a discrete convection operator (to be understood as "the discrete counterpart of a first order conservative differential operator") to enjoy this property. The second result states a convergence result which is useful to check these assumptions, namely the convergence to zero of "discrete time and space tranlates" (see below for a definition) of a converging sequence of functions in L^1. We write these theorem with specific notations for the space and time discretizations.

A.1. **Consistency results**

The discrete convection operator that we consider here takes the following form:

$$\begin{aligned} \mathcal{C}(U):\quad & \Omega \times (0,T) \to \mathbb{R}, \\ & (\boldsymbol{x}, t) \mapsto \mathcal{C}(U)^n_P, \qquad \text{for } \boldsymbol{x} \in P,\ P \in \mathcal{P},\ \text{and } t \in (t_n, t_{n+1}),\ n \in [\![0, N-1]\!], \end{aligned}$$

with

$$\mathcal{C}(U)^n_P = \frac{\beta^{n+1}_P - \beta^n_P}{\delta t} + \frac{1}{|P|} \sum_{\zeta \in \mathfrak{F}(P)} |\zeta|\ \boldsymbol{F}^n_\zeta \cdot \boldsymbol{n}_{P,\zeta},$$

where $\{\beta^n_P,\ P \in \mathcal{P},\ n \in [\![0, N]\!]\}$ is a family of real numbers, $\{\boldsymbol{F}^n_\zeta,\ \zeta \in \mathfrak{F},\ n \in [\![0, N-1]\!]\}$ is a family of real vectors of $\mathbb{R}^d$ and $\boldsymbol{n}_{P,\zeta}$ stands for the normal vector to ζ pointing outward P. Note that this form of the flux implies that the scheme is conservative. Of course, the real numbers $\{\beta^n_P,\ P \in \mathcal{P},\ n \in [\![0, N]\!]\}$ and $\{\boldsymbol{F}^n_\zeta,\ \zeta \in \mathfrak{F},\ n \in [\![0, N-1]\!]\}$ are related to the unknown U.

The consistency of this discrete convection operator is proven in [9, Theorem 2.1], which also states the assumptions that must be satisfied by the above defined quantities to ensure the consistency of the discrete convection operator $\mathcal{C}(U)$. Unfortunately we cannot apply it directly in the framework of our paper, since the third assumptions of this theorem involves a normal flux on the faces of the dual mesh, which are in general not defined in the schemes we are studying. To overcome this difficulty, we use two intermediate results of [9, Theorem 2.1]. The first one, [9, Lemma 2.7], deals with the consistency of the discrete time derivative; it is used in Section 4 with the dual mesh to show the consistency of the time derivative of the momentum. The second one, [9, Lemma 2.8] deals with the consistency of the nonlinear divergence term in the momentum equation, and is used in Section 4 with the primal mesh because of the non existence of normal vectors for general dual meshes. These two lemmas require the following common assumptions: for a sequence $(\mathcal{P}^{(m)}, \mathcal{T}^{(m)})_{m\in\mathbb{N}}$ of space-time discretisations, with $\delta(\mathcal{P}^{(m)}), \delta t^{(m)} \to 0$ as $m \to +\infty$, let $(U^{(m)})_{m\in\mathbb{N}}$ be the associated sequence of discrete functions. We suppose that the sequence $(U^{(m)})_{m\in\mathbb{N}}$ is bounded and converges to a limit: there exists $C_5 \in \mathbb{R}_+^*$ such that

$$\|U^{(m)}\|_{L^\infty(\Omega\times(0,T),\mathbb{R}^p)} \le C_5, \ \forall m \in \mathbb{N}, \tag{53a}$$

$$\exists\, \bar{U} \in L^\infty(\Omega\times(0,T),\mathbb{R}^p) \text{ s.t. } \|U^{(m)} - \bar{U}\|_{L^1(\Omega\times(0,T),\mathbb{R}^p)} \to 0 \text{ as } m \to +\infty. \tag{53b}$$

Lemma A.1 (LW-consistency, time derivative)**.** *Assuming* (51)*, let* $(\mathcal{P}^{(m)}, \mathcal{T}^{(m)})_{m\in\mathbb{N}}$ *be a sequence of space-time discretisations, with* $\delta(\mathcal{P}^{(m)})$ *and* $\delta t^{(m)}$ *tending to zero as* $m \to +\infty$*, and let* $(U^{(m)})_{m\in\mathbb{N}}$ *be the associated sequence of discrete functions satisying* (53)*. Let* $U_0 \in L^\infty(\Omega,\mathbb{R}^p)$ *and assume that*

$$\sum_{P\in\mathcal{P}_{\rm int}^{(m)}} \int_P |(\beta^{(m)})_P^0 - \beta(U_0(\boldsymbol{x}))|\,\mathrm{d}\boldsymbol{x} \to 0 \ \textit{as}\ m \to +\infty, \tag{54}$$

$$\sum_{n=0}^{N_m-1} \sum_{P\in\mathcal{P}_{\rm int}^{(m)}} \int_{t_n}^{t_{n+1}} \int_P |(\beta^{(m)})_P^n - \beta(U^{(m)}(\boldsymbol{x},t))|\,\mathrm{d}\boldsymbol{x}\,\mathrm{d}t \to 0 \ \textit{as}\ m \to +\infty, \tag{55}$$

where $\mathcal{P}_{\rm int}^{(m)}$ *denotes the set of cells of* $\mathcal{P}^{(m)}$ *that have no face or edge on the boundary* $\partial\Omega$*. Then*

$$\sum_{n=0}^{N^{(m)}-1} \sum_{P\in\mathcal{P}^{(m)}} |P| \left((\beta^{(m)})_P^{n+1} - (\beta^{(m)})_P^n\right) \varphi_P^n \to -\int_\Omega \beta(U_0)(\boldsymbol{x})\ \varphi(\boldsymbol{x},0)\,\mathrm{d}\boldsymbol{x} - \int_0^T \int_\Omega \beta(\bar{U})(\boldsymbol{x},t)\ \partial_t\varphi(\boldsymbol{x},t)\,\mathrm{d}\boldsymbol{x}\,\mathrm{d}t \quad \textit{as}\ m \to +\infty,$$

with

$$\varphi_P^n = \frac{1}{|P|}\int_P \varphi(\boldsymbol{x},t_n)\,\mathrm{d}\boldsymbol{x}. \tag{56}$$

Lemma A.2 (LW-consistency, space derivative)**.** *Assuming* (51)*, let* $(\mathcal{P}^{(m)}, \mathcal{T}^{(m)})_{m\in\mathbb{N}}$ *be a sequence of space-time discretisations, with* $\delta(\mathcal{P}^{(m)})$ *and* $\delta t^{(m)}$ *tending to zero as* $m \to +\infty$*, and let* $(U^{(m)})_{m\in\mathbb{N}}$ *be the associated sequence of discrete functions safisying* (53)*. Assume furthermore that*

$$\sum_{n=0}^{N^{(m)}-1} \sum_{P\in\mathcal{P}_{\rm int}^{(m)}} \frac{\mathrm{diam}(P)}{|P|} \sum_{\zeta\in\mathfrak{F}(P)} |\zeta| \int_{t_n}^{t_{n+1}} \int_P |((\boldsymbol{F}^{(m)})_\zeta^n - \boldsymbol{f}(U^m(\boldsymbol{x},t)))\cdot\boldsymbol{n}_{P,\zeta}|\,\mathrm{d}\boldsymbol{x}\,\mathrm{d}t \to 0, \tag{57}$$

Then

$$\sum_{n=0}^{N^{(m)}-1} \delta t^{(m)} \sum_{P\in\mathcal{P}^{(m)}} \sum_{\zeta\in\mathfrak{F}(P)} |\zeta|\ (\boldsymbol{F}^{(m)})^n_\zeta \cdot \boldsymbol{n}_{P,\zeta}\ \varphi^n_P \to -\int_0^T \int_\Omega \boldsymbol{f}(\bar{U})(\boldsymbol{x},t)\cdot\boldsymbol{\nabla}\varphi(\boldsymbol{x},t)\,\mathrm{d}\boldsymbol{x}\,\mathrm{d}t \quad \text{as } m\to+\infty,$$

with φ^n_P *defined by* (56).

If both the assumptions of Lemma A.1 and Lemma A.2 are satisfied, then the convergence of the weak form of the whole discrete convection operator is ensured, see [9, Theorem 2.1]. However, in our setting, the assumption (57) of Lemma A.2 cannot be satisfied on virtual dual meshes, so that Lemma A.1 is used on the dual mesh (it does not necessitate the knowledge of the boundaries of the dual cells) while Lemma A.2 is used on the primal mesh, for which the assumption 57 can be checked.

A.2. **A bound of discrete translates of discrete functions**

The following result is a consequence of [9, Lemma A.1]. It features a mesh $\mathcal{P}$ which can be either the primal mesh, the dual mesh, or a mesh constructed from the edges of the dual mesh. For $u\in L^1(\Omega\times(0,T))$, $P\in\mathcal{P}$ and n such that $n\in[\![0,N-1]\!]$, let u^n_P be the mean value of u over $P\times(t_n,t_{n+1})$. Let $T_\mathcal{P}\,u$ be defined by

$$T_\mathcal{P}\,u = \sum_{n=0}^{N-1}\delta t \sum_{\sigma=P|Q\in\mathcal{E}(\mathcal{P})} \omega_{P,Q}\ |u^{n+1}_Q - u^{n+1}_P| \tag{58}$$

where $(\omega_{P,Q})_{\sigma=P|Q\in\mathcal{E}(\mathcal{P})}$ is a set of non-negative weights. We introduce the two following parameter:

$$\theta_\mathcal{P} = \max_{P\in\mathcal{P}} \frac{1}{|P|} \sum_{\substack{Q\in\mathcal{P}\\ \{P,Q\}\in\mathcal{S}_x}} \omega_{P,Q}. \tag{59}$$

Theorem A.3. *Let* $(\mathcal{P}^{(m)})_{m\in\mathbb{N}}$ *be a given sequence of meshes with* $h^{(m)}=\max_{K\in\mathcal{P}^{(m)}}\to 0$ *as* $m\to+\infty$*, and let* $\delta t^{(m)}\to 0$*as* $m\to+\infty$*. Let us suppose that there exists* $\theta>0$ *such that* $\theta_{\mathcal{P}^{(m)}}\le\theta$ *for all* $m\in\mathbb{N}$*, with* $\theta_{\mathcal{P}^{(m)}}$ *by Equation* (59)*.*

Let $u\in L^1(\Omega\times(0,T))$ *and* $(u_p)_{p\in\mathbb{N}}$ *be a sequence of functions of* $L^1(\Omega\times(0,T))$ *such that* $u_p\to u$ *in* $L^1(\Omega\times(0,T))$ *as* $p\to+\infty$*.*

Then $T_{\mathcal{P}^{(m)}}\,u_p$ *defined by* (58) *tends to zero when* m *tends to* $+\infty$ *uniformly with respect to* $p\in\mathbb{N}$*.*

References

[1] G. Ansanay-Alex, F. Babik, J.-C. Latché, and D. Vola. An L2-stable approximation of the Navier-Stokes convection operator for low-order non-conforming finite elements. *International Journal for Numerical Methods in Fluids*, 66:555–580, 2011.

[2] F. Babik, J.-C. Latché, B. Piar, and K. Saleh. A staggered scheme with non-conforming refinement for the navier-stokes equations. In J. Fuhrmann, M. Ohlberger, and C. Rohde, editors, *Finite Volumes for Complex Applications VII-Methods and Theoretical Aspects*, pages 87–95, Cham, 2014. Springer International Publishing.

[3] T. Baudouin, J.-F. Remacle, E. Marchandise, F. Henrotte, and C. Geuzaine. A frontal approach to hex-dominant mesh generation. *Adv. Model. and Simul. in Eng. Sci.*, 66, 2014.

[4] R. Biswas and R. C. Strawn. Tetrahedral and hexahedral mesh adaptation for CFD problems. *Applied Numerical Mathematics*, 26(1):135–151, 1998.

[5] A. Brunel, R. Herbin, and J.-C. Latché. A MUSCL-like finite volumes approximation of the momentum convection operator for low-order nonconforming face-centred discretizations. *Manuscript in preparation*, 2022.

[6] CALIF^{3}S. A software components library for the computation of fluid flows. `https://gforge.irsn.fr/gf/project/califs`.
[7] T. Gallouët, L. Gastaldo, R. Herbin, and J.-C. Latché. An unconditionally stable pressure correction scheme for compressible barotropic Navier-Stokes equations. *Mathematical Modelling and Numerical Analysis*, 42:303–331, 2008.
[8] T. Gallouët, R. Herbin, and Latché. On the weak consistency of finite volume schemes for conservation laws on general meshes. *SeMA Journal*, 76:581–594, 2019.
[9] T. Gallouët, R. Herbin, and J.-C. Latché. Lax-Wendroff consistency of finite volume schemes for systems of non linear conservation laws: extension to staggered schemes. *SeMA Journal*, 79:333354, 2022.
[10] L. Gastaldo, R. Herbin, J.-C. Latché, and N. Therme. A MUSCL-type segregated–explicit staggered scheme for the Euler equations. *Computers & Fluids*, 175:91–110, 2018.
[11] R. Herbin, W. Kheriji, and J.-C. Latché. On some implicit and semi-implicit staggered schemes for the shallow water and Euler equations. *Mathematical Modelling and Numerical Analysis*, 48:1807–1857, 2014.
[12] R. Herbin, J.-C. Latché, S. Minjeaud, and N. Therme. Conservativity and weak consistency of a class of staggered finite volume methods for the Euler equations. *Mathematics of Computation*, on line 2020.
[13] R. Herbin, J.-C. Latché, and T. Nguyen. Consistent segregated staggered schemes with explicit steps for the isentropic and full Euler equations. *Mathematical Modelling and Numerical Analysis*, 52:893–944, 2018.
[14] J.-C. Latché and K. Saleh. A convergent staggered scheme for the variable density incompressible Navier-Stokes equations. *Mathematics of Computation*, 87:581–632, 2018.
[15] M.-S. Liou. A sequel to AUSM, part ii: AUSM+-up for all speeds. *Journal of Computational Physics*, 214(1):137–170, 2006.
[16] M.-S. Liou and C. J. Steffen. A new flux splitting scheme. *Journal of Computational Physics*, 107(1):23–39, 1993.
[17] D. J. Mavriplis and V. Venkatakrishnan. A unified multigrid solver for the Navier-Stokes equations on mixed element meshes. *International Journal of Computational Fluid Dynamics*, 8(4):247–263, 1997.
[18] S. J. Owen and S. Saigal. Formation of pyramid elements for hexahedra to tetrahedra transitions. *Computer Methods in Applied Mechanics and Engineering*, 190(34):4505–4518, 2001.
[19] J. L. Steger and R. F. Warming. Flux Vector Splitting of the Inviscid Gasdynamic Equations with Application to Finite Difference Methods. *Journal of Computational Physics*, 40(2):263–293, Apr. 1981.
[20] K. Sørensen, O. Hassan, K. Morgan, and N. P. Weatherill. A multigrid accelerated hybrid unstructured mesh method for 3d compressible turbulent flow. *Computational Mechanics*, 31:101114, 2003.
[21] E. Toro and M. Vázquez-Cendón. Flux splitting schemes for the Euler equations. *Computers & Fluids*, 70:1–12, 2012.
[22] G.-C. Zha and E. Bilgen. Numerical solutions of Euler equations by using a new flux vector splitting scheme. *International Journal for Numerical Methods in Fluids*, 17(2):115–144, 1993.